BEN-GURION UNIVERSITY OF THE NEGEV
FACULTY OF ENGINEERING SCIENCES
DEPARTMENT OF INDUSTRIAL ENGINEERING AND MANAGEMENT

A Robotic System for Disease Detection in Greenhouse Peppers

THESIS SUBMITTED IN PARTIAL FULFILLMENT OF THE REQUIREMENTS
FOR THE M.Sc. DEGREE

By: Noa Schor

October 2015

BEN-GURION UNIVERSITY OF THE NEGEV
FACULTY OF ENGINEERING SCIENCES
DEPARTMENT OF INDUSTRIAL ENGINEERING AND MANAGEMENT

A Robotic System for Disease Detection in Greenhouse Peppers

THESIS SUBMITTED IN PARTIAL FULFILLMENT OF THE REQUIREMENTS FOR THE M.Sc. DEGREE

By: Noa Schor

Supervised by: Sigal Berman
Avital Bechar

Author: …….. Date: ……..

Supervisor: …… Date: ……..

Supervisor: …… Date: ……..

Chairman of Graduate Studies Committee: …….. Date: …….....

October 2015

Abstract

Robotic systems for plant disease detection in greenhouses enable early detection and improved control. They are expected to increase yield, improve quality, reduce pesticide application, increase sustainability, and reduce costs. Threat symptoms vary per each disease and crop, and each plant suffers from multiple threats, thus, dedicated integrated disease detection systems and algorithms are required. We present a robotic system for disease detection for greenhouse bell peppers developed using a holistic approach, integrating design of motion and perception for two major threats of greenhouse bell peppers: powdery mildew (PM) and *Tomato spotted wilt virus* (TSWV). The detection system comprises a mechanical structure, a sensor suite, motion planning, and disease detection algorithms. Visual spectrum imagery is used for motion planning and disease detection for fast, non-destructive, and cost effective operation. An algorithm based on principal component analysis (PCA) was developed for PM, and three algorithms were developed for TSWV detection, one based on PCA and two on the coefficient of variation (CV). The algorithms were tested using images of healthy and infected plants taken in a greenhouse. For RGB-based detection, for TSWV, PCA-based classification with leaf veins removal, achieved the highest classification accuracy (90%), yet the accuracy of the CV methods was also high (85%, 87%). For PM, pixel-level classification accuracy was high (95.2%) while leaf condition classification accuracy was low (64.3%) since leaf images were acquired from the top part of the leaf while disease symptoms start appearing on its bottom part. NIR-R-G-based detection achieved inferior results for both diseases. The components of the system were integrated and preliminary integration tests were conducted in a laboratory environment to verify that all system components indeed work together. The integrated system operated successfully for

110 consecutive minutes with an average cycle time of 26.7 sec for end-effector velocity of 15 mm/sec and PCA-based detection algorithms. Future research will examine improvement of disease detection, aiming to achieve higher accuracy along with earlier detection, e.g., by facilitating PM examination in the bottom side of the leaf or by integration of the two CV-based methods. For complete integration tests and field performance studies, a dynamic detection process (i.e., with a moving conveyor) will be implemented and tested.

Key words

Agricultural automation, Computer vision for automation, Robotic disease detection system, Disease detection, *Tomato spotted wilt virus*, PM, Classification, Principal component analysis, Coefficient of variation, Greenhouse bell pepper crop.

Acknowledgements

It is a pleasure to thank those who have made this thesis possible. I would like to thank my supervisors, Sigal Berman and Avital Bechar, for their patience, motivation, enthusiasm and professional guidance throughout the last two years.

Many thanks to my colleagues at the Agricultural Robotics Lab in the Institute of Agricultural Engineering - Timea Ignat, Sivan Levi, Guy Lidor, Victor Bloch, Roee Finkelshtain and Yossi Portal who have given me their time, wisdom and patience. Timea has given her insights and advices through the development of the PCA-based classification algorithm, without her ideas and guidance the algorithm was not taking shape. Sivan has helped me with the physical system development as developed the custom made end-effector and placed all necessary sensors on it. Guy has helped me a lot to operate the NIR-R-G camera and helped with the mechanical design of the apparatus for data collection. Victor has made himself available and taught me how to use the manipulator. Roee has contributed his experience and creativity and helped solve problems as emerged during development. Yossi has cultivated pepper plants making sure they are ready whenever they are needed, even out of season.

A special thanks to Aviv Dombrovsky and Yigal Elad from the Department of Plant Protection at the Volcani Center for their professional guidance and patience through diseases symptoms ground truth establishment. Thanks to Dalia Rav-David and Oded Lachman for ensuring the healthy status of pepper plants and the normal disease development.

Last but not least, I would like to thank my family- my husband Gal, my parents Razia and Ofer and my brother and sister Nadav and Yael who have endured countless hours of working and studying and who have supported me with their love.

Content

Abbreviations

CV	coefficient of variation
CV^b	green coefficient of variation
CV^g	blue coefficient of variation
CV^r	red coefficient of variation
DoF	degrees-of-freedom
DP	ratio of diseased pixels
EC	electrical conductivity of water
ELISA	enzyme-linked immunosorbent assay
FN	false negative
FP	false positive
LB	lower bound
LDA	linear discriminant analysis
NPK	nitrogen, phosphorus and potassium
PCA	principal component analysis
PM	powdery mildew
pose	position and orientation
QDA	quadratic discriminant analysis
TCP	tool center point
TH	healthy threshold
TN	true negative
TP	true positive
TS	severity threshold
TSWV	*Tomato spotted wilt virus*
UB	upper bound

Tables

Figures

1. Introduction

1.1. Problem definition

Traditional agricultural management practices assume that the parameters of crop growing fields are homogeneous (Steiner et al., 2008). In contrast, modern, precision agriculture integrates different technologies, such as: sensors and information and management systems for adapting agricultural practices to parameter variability within the field (McBratney et al., 2005; Dong et al., 2013 a). Monitoring is a major field within realm of precision agriculture and a paramount component of precision crop protection (Gebbers and Adamchuk, 2010; Schellberg et al., 2008).

Crop yield is affected by different stresses, e.g., pests, diseases, weed, environmental conditions, nutrition or water deficiencies, which can impair the production capacity. Oerke and Dehne (2004) indicated that the impact of diseases, insects, and weeds represents a potential annual loss of 40% of world food production. Since the occurrence of diseases depends on environmental factors and as diseases often exhibit a sporadic spatial distribution, sensing techniques can be useful in identifying primary disease foci and distribution (Franke and Menz, 2007; Franke et al., 2009). Sankaran et al. (2010) and Lee et al. (2010) suggested that detection and quantification of diseases based on visible and infrared spectroscopy would be feasible. As if a symptom or a disease is detectable by naked eye, it should be measurable with a sensor, recording the stress symptoms (Nutter et al., 1990; Stafford, 2000).

Currently, disease detection and monitoring in greenhouses are conducted manually by an expert inspector and are limited due to human resources availability, low sampling rate and high monitoring costs. Sampling rate and resolution are low with

about 20 arbitrarily locations sampled per hectare in a fixed pattern (the same locations are revisited) and each plot is monitored every 7-10 days. The plants are inspected for symptoms by an inspector crossing the greenhouse rows on foot. Thus the inspector walks about 20 km per day covering about 8 hectares and a designated inspector is required for every 80 hectares. The limitations of the current inspection methods can lead to late detection and inability to contain a disease. As a precaution, repeated, high doses of pesticide are often applied even when symptoms are far below thresholds which mandate pesticide application. Moreover pesticides are typically applied uniformly throughout the greenhouse while disease distribution is typically centered in distinct locations, resulting in additional pesticides use, increased material cost and environmental impact.

1.2. Research objectives, innovations and contributions

The long term objective of the current research is to construct a robotic detection system for greenhouse bell peppers. The current thesis centered about the design of the system for detecting two major threats of greenhouse bell peppers: PM TSWV using a single mobile system. This required developing suitable image processing algorithms, motion and task planning, and component integration. The importance of the research and the strength of its results are enhanced by the fact that detection algorithms for PM have previously been developed for other crops, but not for peppers, and there are not any known image-based detection algorithms for TSWV. Moreover, detection of several diseases in pepper plants using a single detection system has not been previously reported. The main innovations of the current work are:

- Development of image-based detection algorithms for PM and TSWV suitable for a mobile robotic system.

- Development of a detection system prototype for two major greenhouse bell pepper diseases, including mechanical structure, sensor suite, motion planning and diseases detection.

The main findings of this thesis have been presented (or are under review) in:

- Schor, N., Bechar, A., Ignat T., Dombrovsky, A., Elad, Y. and Berman, S., "Robotic Disease Detection in Greenhouses: PM and Tomato Spotted Wilt Virus Identification," *IEEE Robotics and Automation Letters* with *IEEE International Conference on Robotics and Automation*, submitted for publication.
- Schor, N., Berman, S., Dombrovsky, A., Elad, Y., Ignat T. and Bechar, A., "A robotic monitoring system for diseases of pepper in greenhouse," in Proc. *10th Euro. Conf. Precision Agriculture (ECPA)*, Israel, 2015, pp. 627-634.
- Schor, N., Berman, S., Dombrovsky, A., Elad, Y., Ignat T. and Bechar, A., "A robotic monitoring system for diseases of pepper in greenhouse," *The Annual Meeting of the Israeli Society of Agricultural Engineering*, Israel, 2015. (Oral presentation)
- Schor, N., Berman, S. and Bechar A., "Motion Planning for a Manipulator in Agriculture," *ABC Robotics Second Meeting of the Executive Steering Committee*, Israel, 2015. (Poster)
- A paper for the Precision Agriculture journal (affiliated with the ECPA conference) is currently in advanced writing stages.

1.3. Scope and limitations

Detection algorithms based on images taken in a greenhouse (rather than a lab) have been developed in order to ensure algorithm suitability for robotic detection system in the field. For PM a detection algorithm based on principal component analysis (PCA) was developed. As this is the first research targeting TSWV detection three different detection algorithms were developed: a PCA-based algorithm and two algorithm variants based on the coefficient of variation (CV) of the symptom pattern. A robotic detection system prototype has been developed, where the sensor

apparatus was mounted on a robot manipulator currently without a mobile platform. The detection algorithms and the robotic system were integrated and preliminary integrations tests were conducted.

This is the first reported disease detection system to target detection of multiple threats, yet currently only two out of multiple threats of greenhouse bell peppers are detected. However, the selected diseases (TSWV and PM) are among the major threats to greenhouse bell peppers. The image databases were constructed in a greenhouse environment with a high resolution RGB camera, not the RGB camera fitted on the robot which is of lower resolution. Future work will determine if and what adaptations may be required to the algorithm or apparatus due to this reduced resolution. The target of the integration test was to verify that all system components indeed work in concert, thus only healthy plants were analyzed. Future work will thoroughly test the complete system in both laboratory and field setups. Yet this was out of scope in the current stage.

1.4. Thesis outline

The rest of this thesis is organized as follows: chapter 2 contains the scientific review regarding precision monitoring, diseases in pepper and their detection techniques; The robotic detection system, which is described in chapter 3, includes apparatus and detection process; chapter 4 presents PM and TSWV detection methods, detection algorithms, experiment conducted for testing the algorithms, results and discussion; preliminary prototype integration described in chapter 5; conclusions and directions for future research are discussed in chapter 6.

2. Literature review

2.1. Precision robotics monitoring of plant diseases

In the last three decades, much work has been done in the field of agricultural robotics and automation, aiming to improve yield quality and reduce operation costs (Foglia and Reina, 2006). Agricultural robotic systems operate in a dynamic environment with elements of uncertainty and lack of information, therefore must be equipped with sophisticated sensing capabilities and advanced motion planning and control (Edan et al., 2000). Moreover the terrain may be difficult for traversing and thus impose the need for various mobility platforms along with sophisticated navigation techniques (Kavraki and LaValle, 2008). Research worldwide has demonstrated the technical feasibility of agricultural robots for a variety of crops, such as tomato (Ryu et al., 2001; Monta et al., 1998), apple (Baeten et al., 2008; Bulanon et al., 2002), cucumber (Van Henten et al., 2006) and pepper (Baur et al., 2012; Qiao et al., 2005; Bac et al., 2013). Common agricultural tasks that have been investigated include transplanting (Huang and Lee, 2008; Parish, 2005; Nagasaka et al., 2007), harvesting (Mann et al., 2014; Bac et al., 2014; Van Henten et al., 2009), guidance and navigation in agricultural environments (Galceran and Carreras, 2013; Bochtis et al., 2010; Dong et al., 2013 b), fruit and vegetable grasping (Kondo et al., 2010; Kubota et al., 2008), irrigation (Miranda et al., 2005) and plant protection and weed control (Bakker et al., 2010; Moshou et al., 2011; Blasco et al., 2002).

Robotic monitoring systems for disease detection can facilitate targeted and timely disease control which can lead to increased yield, improved crop quality, and massive reduction in the quantity of applied pesticides (Bock et al., 2010). In addition to reduced production costs, this will also lead to reduced exposure to

pesticides of farm workers and inspectors, and increased sustainability (Hillnhuetter and Mahlein, 2008). Mobile robotic manipulators with various sensing capabilities can offer an automation solution suitable for disease detection in greenhouses. However, comprehensive research on the development of such integrated robotic disease detection systems for greenhouses is sparse, probably, as the preliminary challenge of development of robust disease detection algorithms is still an open research question. Aerial platforms (Gennaro et al., 2012) and ground mobile robotic platforms with fixed sensor configurations (Moshou et al., 2011; Pilli et al., 2014) for disease detection have been tested for open field crops. Yet, in greenhouses both solutions have inherent shortcomings. The maneuverability and flight duration of aerial systems within greenhouses is limited, and navigation and localization cannot rely on GPS sensors since the construction can cause unpredictable position errors, therefore their main advantages are irrelevant. In greenhouses, pose adaptation can significantly improve detection, especially early detection, when symptoms are typically centered in distinct locations. For fixed sensor configuration pose adaptation is not possible. Moreover in fixed configuration systems multiple disease detection can lead to a requirement for multiple detection poses which tends to increase system complexity and cost and hinder maneuverability. Therefore the developed robotic disease detection system for greenhouse pepper plants is based on the concept of a mobile robotic manipulator (Schor et al., 2015; Schor et al., submitted a) which offers the required maneuverability and flexibility.

2.1.1. Image processing for disease detection

Vision-based sensors for disease detection have many advantages, as they collect spatial information, offer non-destructive and fast detection capabilities along with low weight and dimensions and thus simple system integration (Sankaran et al.,

2010). Disease detection based on electromagnetic vision systems, i.e., image processing, is based on the hypothesis that the electromagnetic reflectance of diseased plants is different than healthy plants. As any disease that causes plant stress which alters foliage radiation reflectance characteristics can be detected using imagery (Sankaran et al., 2010; Lee et al., 2010), researchers have applied image processing techniques to detect, quantify, and classify various plant diseases in many different cultivars (for reviews see: Barbedo and Garcia, 2013; Pujari et al., 2015; Patil and Kumar, 2011; Lee et al., 2010). Various classification methods have been used, e.g., principal component analysis (PCA) (Schor et al., submitted b; Pagola et al., 2009), neural networks (Moshou et al., 2011), and support vector machines (Rumpf et al., 2010). These methods were applied to data from various spectrum ranges.

Plant diseases can affect various optical foliage characteristics therefore disease detection can be based on different spectral ranges (Lee et al., 2010). In the visual spectrum (400–700 nm) healthy leaves exhibit low reflectance due to strong absorption by photoactive pigments. Due to the characteristics of these pigments in healthy leaves, green is typically the most efficiently reflected visual-range band. Diseases commonly induce discrete lesions on the leaves due to necrotic or chlorotic regions which increases visual spectrum reflection. In the near infrared (NIR) band (700–1200 nm) healthy plants exhibit high reflectance due to the internal structure of the leaf tissue. Plant diseases lead to reduction in biomass due to cellular senescence, reduced growth, and defoliation which decrease NIR reflectance. In the short wave infrared (SWIR) band (1200–2500 nm) water, proteins, and other carbon constituents lead to low reflectance in healthy plants. Lack of these ingredients caused by disease leads to increased reflectance in infected plants. Methods based on fluoresce or

thermography can also be used for disease detection and have been extensively studied, yet they are less relevant for a robotic detection system operating in the field due to cost, payload weight, and required setup.

2.2. Diseases detection of peppers

Bell pepper (*Capsicum annuum*) is a specialty, high-value crop, grown mostly in greenhouses for fresh markets. It is cultivated worldwide and used as food ingredient, spice, and as an ingredient in medicine. Pernezny et al. (2003) provides a comprehensive presentation of different pepper diseases caused by infectious agents; diseases caused by bacteria (e.g., Bacterial spot, Bacterial Canker and Bacterial wilt), fungi and oomycetes (e.g., PM, Damping-off, Fusarium wilt and Phytophthora Blight), viruses (e.g., Tomato spotted wilt virus, Cucumber mosaic virus and Potato virus Y), angiosperm (e.g., Dodder), or nematodes (e.g., Root-knot nematodes). Among all the threats listed above, TSWV and PM fungi (Fig. 2.1) are the most damaging in their respective category (viral and fungi) and both have severe consequences to the fruit and the leaves. Detection of these threats during a single pass of a robotic system is challenging as their characteristics differ in visible symptoms and in outbreak regions.

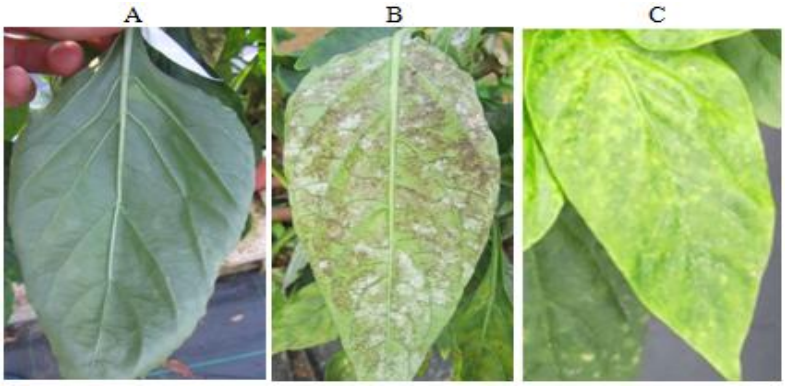

Figure 2.1. Pepper leaves. A. Healthy; B. Powdery mildew; C. *Tomato spotted wilt virus* (Schor et al., submitted a)

2.2.1. *Tomato spotted wilt virus* (TSWV)

TSWV (Fig. 2.1C) was first observed in 1915 in Australia and described as the "spotted wilt" of tomatoes (Brittlebank, 1919) that later was associated with transmission by thrips (Pittman, 1927). TSWV is transmitted by eight species of thrips (e.g., western flower thrips *Frankliniella occidentalis*) (Pernezny et al., 2003) in a persistent and propagative manner (Fereres and Raccah, 2015). TSWV outbreaks are difficult to manage making it a major threat in many vegetable production areas, e.g., tomato, tobacco, lettuce, pepper, papaya, eggplant, green beans, artichokes, broad beans, celery, and more. Over 1000 plants species experience severe losses due to the virus (Prins and Goldbach, 1998; Rosella et al., 1996). In pepper plants, TSWV causes a range of symptoms: sudden yellowing, mild mottling, mosaic, browning of young leaves on the upper part of the plant which later become necrotic, and occasionally ring-shaped spots which appear on both leaves and fruits. TSWV causes heavy crop losses since fruit formed after infection display large necrotic streaks and spots while younger fruit may become totally necrotic (Avila et al., 2006). Early detection of TSWV in pepper plants is crucial as it has only recently overcome plant resistance (Crescenzi et al., 2013; Sharman and Persley, 2006; Margaria et al., 2004; Roggero et al., 2002). Currently there is no treatment for TSWV in peppers, and thus infected plants must be terminated as soon as possible.

TSWV detection has been studied using chemical sensors, e.g., ELISA (enzyme-linked immunosorbent assay) (Crescenzi et al., 2013; Avila et al., 2006). Such methods are destructive as leaves must be extracted from the plant. An additional disadvantage of these methods is that the selection of samples to be tested has crucial influence on method reliability due to uneven distribution of TSWV in the

greenhouse. To our best knowledge, there are currently no image-based detection algorithms for TSWV. Therefore one of the main innovations in the current work is the development of such algorithms.

2.2.2. Powdery mildew (PM)

PM (Fig. 2.1B), caused by the fungus *Leveillula taurica*, is a serious threat to a very wide host range such as, onions, chickpea, potatoes, weed and pepper. Its effected plant list extends to more than 1000 plant species (Zheng et al., 2013; Glawe et al., 2010; Attanayake et al., 2008; Du Toit et al., 2004; Glawe et al., 2004). Economic losses specifically yield loss of 2-4 kg/m^2 were reported on greenhouse pepper in British Columbia in 2002 due to heavy epidemics of PM (Cerkauskas and Buonassisi, 2003). Studies conducted in greenhouses and fields showed that leaves infected by PM shed prematurely, resulting in a reduced photosynthetic area, inhibition of fruit development, reduction in the number of flowers per plant, and increased sunburn damage to exposed fruit (Smith et al., 1999; Elad et al., 2007). Pernezny et al. (2003) described the visible symptoms of PM in peppers as yellow-brown spots with whitish powdery mycelium which typically appear first on the underside of older and lower leaves.

Imaged-based detection algorithms have been developed for PM in wheat (Franke and Menz, 2007) and grapevine (Belanger et al., 2008; Oberti et al., 2014) using UV (Belanger et al., 2008) and multispectral camera (Oberti et al., 2014; Franke and Menz, 2007). These and additional methods are reviewed in Table 2.1. Belanger et al. (2008) have applied UV-induced fluorescence measurements to detect and quantify PM infection symptoms on grapevine leaves by investigating different emission/excitation wavelength combinations, finding that the ratio between blue and green fluorescence intensity of healthy and diseased areas of leaves showed

significantly different results starting from three days after infection. The developed UV-based detection method requires complex fluorescents excitation therefore its implementation outside a laboratory is problematic. Oberti et al. (2014) have investigated how the view angle can affect the detection's sensitivity of PM in grapevine leaves using multispectral imaging. The potential of multispectral remote sensing for PM detection in wheat was presented by Franke and Menz (2007) which achieved maximum classification accuracy of 88%. Yet, the high cost of multispectral imaging systems is prohibiting for deployment in small and medium farms, which is often the case for greenhouse operation. Accordingly, one of the main innovations in the current research is using visible spectrum for PM detection in peppers. Imaging sensors in the visible spectrum tend to be cheap and robust reducing the costs and integration complexity.

Table 2.1. Systems for PM detection

System Type	Enviro-nment	Algorithm	Detection stage	Reference
Laser UV induced fluorescence (non-imaging flurometer)	Lab	Using fluorescence amplitude ratios F451:F522, F522:F687, and F522:F736 of the half-bandwidth.	Early detection 10-12 hr after inoculation	(Burling et al., 2012)
Laser UV induced fluorescence (imaging flurometer with CCD Camera; CoolSnapHQ)	Lab	Image correction, interest area selection, fluorescence ratios computation and edge detection. Least squares to fit general linear models used.	Early detection from 3 days after inoculation	(Belanger et al., 2008)
Digital Imaging (RGB Camera)	Lab	Image processing algorithms	Medium to advanced stage (when visible effects start)	(Vijayakumar and Arumugam, 2012)
Multispectral reflectance (spectrophotometer)	Lab, Field	Filtering, Statistical analysis, Classification techniques (LDA, PCA, PLS).	Medium to advanced disease intensity	(Tirelli et al., 2012)
Hyperspectral imaging system (multispectral camera)	Field	Spatio-temporal analysis, mixture tuned matched filtering (MTMF), vegetation index (NDVI).	Medium to advanced intensity disease	(Franke and Menz, 2007)
Hyperspectral imaging system (spectrometer with CCD Camera; Duncan MS4100)	Green-house, Field	Image processing algorithms, vegetation indices (REIP, RIR, NDVI) and discriminant functions (QDA).	Medium to advanced intensity disease	(Oberti et al., 2012)

3. Detection System

3.1. Robotic disease detection system

The robotic disease detection system developed (Fig. 3.1) includes three components: a robotic manipulator (Fig. 3.2), a custom-made end-effector, and a sensory apparatus. The sensory apparatus comprises an RGB camera (LifeCam NX-6000 WebCam, Microsoft, USA) with a resolution of 1600x1200 pixels, a NIR-R-G camera (ADC Lite, 520-920nm, Tetracam, USA) with a resolution of 2048x1536 pixels, and a single laser beam distance sensor (DT35, SICK, Germany). The sensor devices are mounted on the custom made end-effector which is attached to the six degrees-of-freedom (DoF) industrial manipulator (MH5L, Motoman, Yaskawa, Germany). Parts of the custom-made end-effector were fabricated using a 3D printing system. The parts were designed to align in parallel the sensor devices, making them coaxial with the manipulator tool center point (TCP).

To simulate the movement of the robotic system in a greenhouse plot, the robotic arm was placed near a conveyor belt carrying pots with plants. It will later be mounted on a mobile platform that will drive through the greenhouse aisle.

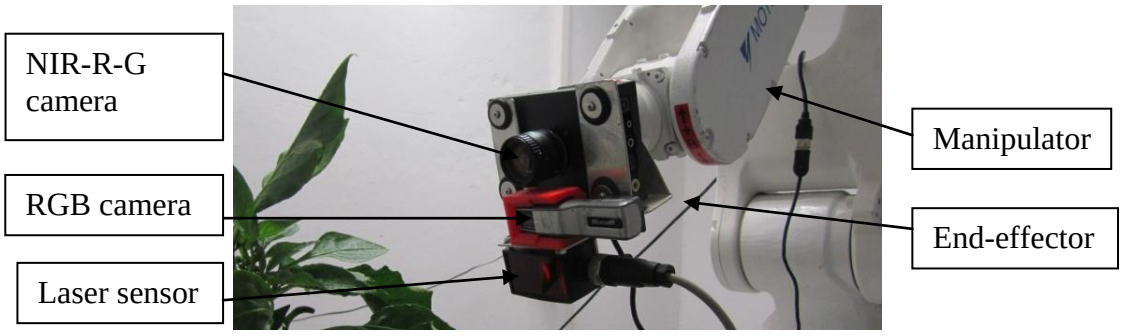

Figure 3.1. The developed robotic detection system (Schor et al., 2015).

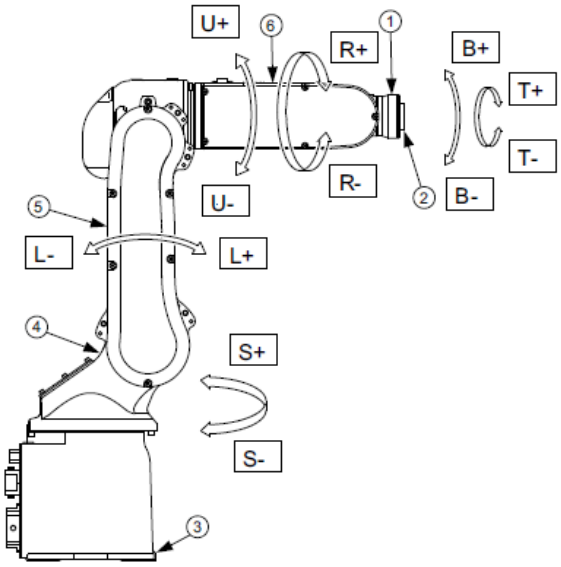

1	Wrist	4	Rotary head
2	Wrist flange	5	Lower arm (L-arm)
3	Robot base	6	Upper arm (U-arm)

Figure 3.2. A scheme of MH5L, a Six DoF industrial manipulator (Motoman, Germany)

3.2. Detection process

To facilitate the required rapid operation, high sampling resolution, and large area coverage, disease detection is done during a single pass of the robot manipulator about the plant. TSWV detection is conducted above the plant and PM detection is conducted alongside the plant. To further shorten operation cycle time, TSWV detection is done first since there is no treatment to TSWV and if it is detected the plant is immediately marked for termination, thus detection of PM for the same plant is not required. The detection process for each disease (Fig. 3.3) is divided into four sub-tasks: i) plant location; ii) determination of the camera position and orientation ('pose'); iii) motion planning execution; and, iv) disease detection.

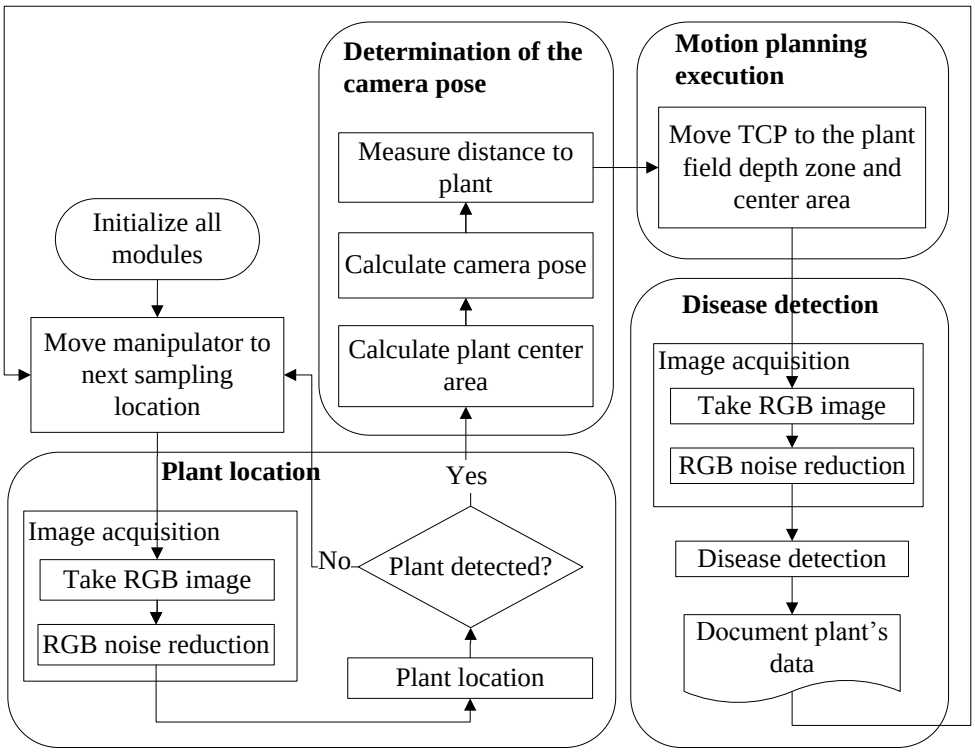

Figure 3.3. Detection process diagram.

Plant location

To locate the plant, the end-effector moves to an initial pose determined a-priori. For TSWV detection the initial pose is above the plant (sensor apparatus facing down) while for PM detection it is alongside the plant (sensor apparatus facing sideways towards the plant). Than an RGB image is acquired and the plant is identified using blob analysis and morphological filters. For blob analysis, 20 healthy leaves were sampled to determine the upper bound (UB) (1) and lower bound (LB) (2) values for each channel R, G and B. The width of standard deviations from the mean (n) was determined to be 2 by trial and error. For this process only healthy leaves were sampled since the detection is expected to be early and most leaves are expected to be not infected.

$$UB_{channel} = mean_{channel} + n * std_{channel} \quad (1)$$

$$LB_{channel} = mean_{channel} - n * std_{channel} \quad (2)$$

A threshold is applied between UB and LB and pixel components are connected and filled to obtain blobs result a binary image of the plant (Fig 3.4).

Figure 3.4. Binary image, calculated by plant location algorithm (left). RGB image, the black box represents the plant center area (right).

Determination of camera pose

The center of the plant, i.e., the center of mass of the green blob, is calculated from the binary image of the plant. The plant center area is defined as an area of 16x16 pixels around the center of the plant (Fig. 3.4). Based on the plant center area and the kinematic model of the system, a pose for performing disease detection is calculated.

Motion planning execution

While the end-effector is moving toward the determined pose, the laser sensor continuously measures distance to adjust the end-effector position (closed-loop control) such that a distance from the plant foliage is set to 210-270 mm facilitating required leaf image resolution. The algorithm was developed under the hypothesis that the closest object to the end-effector is the plant, thus the laser sensor is measuring the distance to the plant foliage (either top or side). Multiple distance measures are executed since a single measurement may miss the plant.

The required pose for performing TSWV detection (Fig. 3.5 a,d) may be situated near singularity point since joints L and U of the manipulator (Fig. 3.2) are fully

aligned. Hence, the inverse kinematic problem cannot be solved analytically for the required pose and a numerical iterative search was implemented. The numerical iterative search objective is to situate the TCP within the plant center area box and it is executed by fixed movements in joints R and B of the manipulator (Fig. 3.2). The direction of the joints movements (left or right and up or down) is determined according the current TCP position regarding the plant center area. In the case of PM detection, the desired pose (Fig. 3.5 c,e) can be directly calculated from the inverse kinematic problem since it is not situated near singularity point.

When the manipulator moves from the TSWV detection pose to the PM detection pose it may collide with the plant. To avoid this, the manipulator moves through an intermediate-point securing motion outside the plant foliage (Fig. 3.5). The motion planner calculates a straight path to and from the intermediate-point using the manipulator's kinematic model.

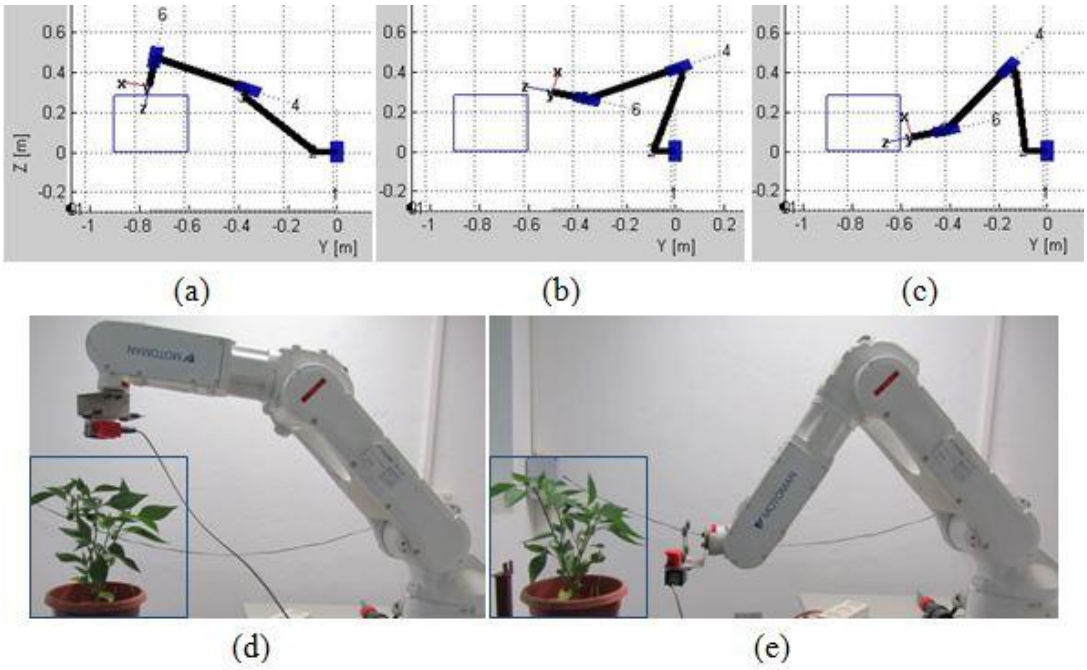

Figure 3.5. Motion planning. (a) and (d) TSWV initial pose; (b) intermediate-point; (c) and (e) PM initial pose. In each sub-graph, the blue solid rectangle represents the plant (obstacle) (Schor et al., 2015).

Disease detection

Once a plant is identified and the camera pose established, the disease detection procedure is initiated. The developed disease detection algorithms are detailed in the following chapter.

4. PM and TSWV detection

4.1. Method

All the detection algorithms developed in this work start with leaf segmentation and removal of background noise based on blob analysis and morphological filters. For PM, a detection algorithm based on principal component analysis (PCA) was developed. For TSWV, as this is the first research targeting TSWV detection, three different detection algorithms were developed: a PCA-based algorithm and two algorithms based on the coefficient of variation (CV) of the symptom pattern.

4.1.1. Principal component analysis

4.1.1.1. RGB-based principal component analysis

In PM the contrast between the symptom and leaf vein color is strong (Fig. 2.1B) while in TSWV the contrast is mild (Fig. 2.1C). Therefore, for TSWV detection a leaf vein extraction algorithm was implemented prior to PCA classification. Preliminary analysis confirmed this stage is required for TSWV and that for PM it is not required. The leaf vein extraction algorithm is based on Savitzky-Golay smoothing and differentiation algorithm (Savitzky and Golay, 1964) followed by multi-level image thresholds using Otsu's method (Otsu, 1979) and morphological filters (e.g., area open and dilate).

A binary classification (healthy or diseased) is conducted at the pixel level of the leaf, based on the two main principal components of the pixel’s R, G, and B values. For determining overall leaf condition, the ratio of the pixels classified as diseased with respect to all pixels in the leaf (DP) is calculated and compared to a healthy threshold value (TH) computed a-priori. Since in the case of TSWV plant termination is required even if severity is low, if DP exceeds TH, the plant is

considered diseased. For PM, severity level determination is required for planning treatment. Therefore the leaf is classified as either healthy or diseased with low severity or diseased with medium severity (DP is compared to severity threshold (TS) in addition to TH). Fig. 4.1 describes PCA-based detection algorithm.

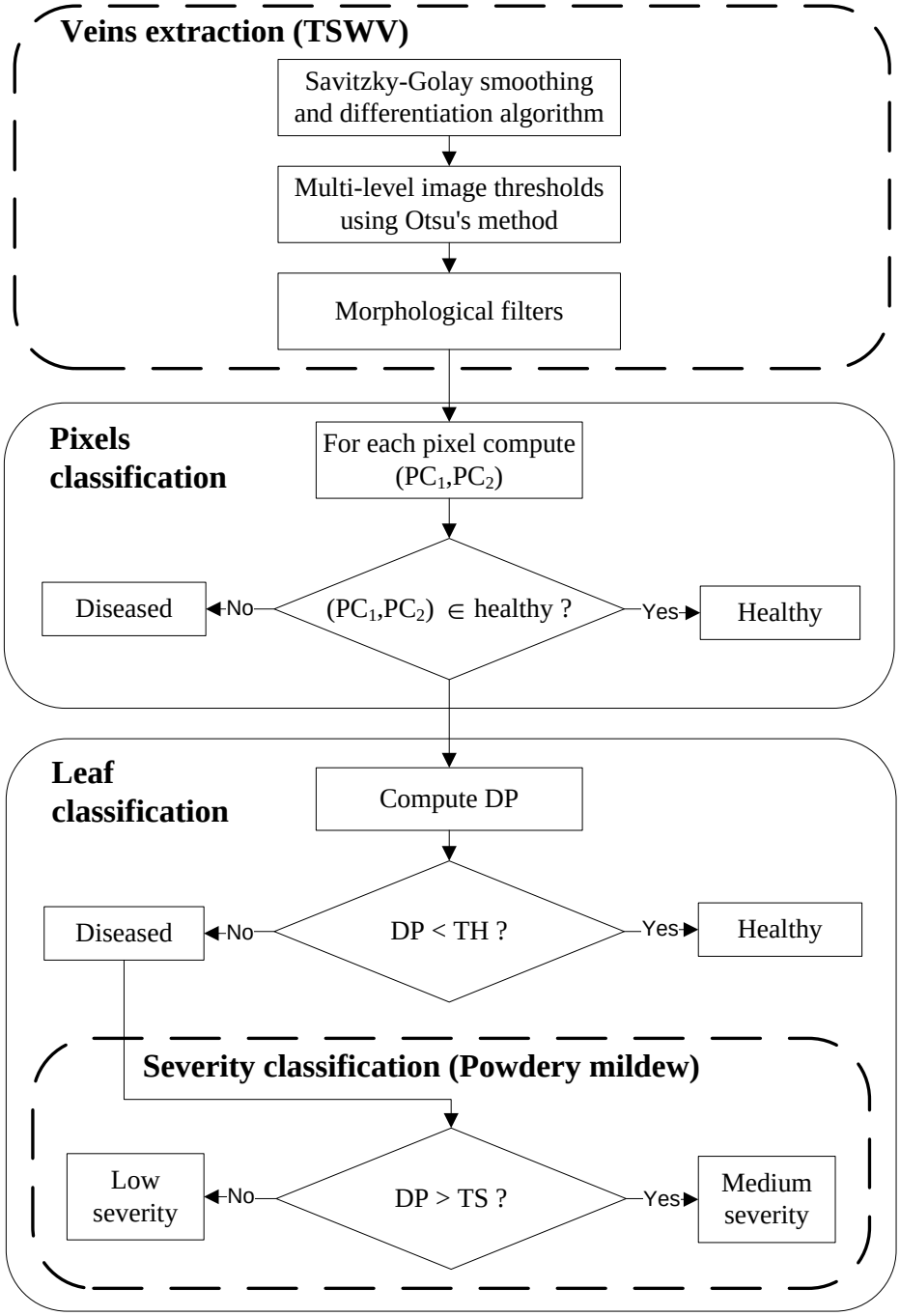

Figure 4.1. PCA-based detection algorithm. DP- ratio of diseased pixels to all pixels in the leaf, TH- healthy threshold, TS- severity threshold (Schor et al., submitted a).

4.1.1.2. NIR-R-G-based principal component analysis

For NIR-R-G imagery, for both PM and TSWV, PCA-based detection algorithms were developed. For pixel level classification the two main principal components of the pixel's NIR, R, and G values were computed. For PM the indices reported by Oberti et al. (2014) were additionally computed and tested. The algorithm stages in all cases are identical to the PCA-based algorithm developed using the RGB-based imagery described in the previous section.

4.1.2. Coefficient of variation of TSWV symptom pattern (RGB-based)

As previously described, TSWV symptoms are characterized by a mosaic pattern, therefore classification based on the CV (Everitt and Skrondal, 1998) was explored (Fig. 4.2). The leaf is scanned by a moving window right-to left, and top-down, and at each step the window is advanced by a single pixel. For each RGB channel, the CV within a window is calculated by dividing the standard deviation of the color value by its mean (red: CV^r, green: CV^g, and blue: CV^b). For all three channels, different window sizes (5x5 to 135x135 pixels in steps of 10) were visually and numerically examined. Based on this examination, two decision rules were defined and implemented (Fig 7): CV^r+CV^b in which the classification decision is based on the values of the average red CV ($\overline{CV^r}$) and the average blue CV ($\overline{CV^b}$) of the same window size; and CV_1^b-CV_2^b in which the classification decision is based on the difference between two $\overline{CV^b}$ values from two window sizes where window 1 is larger window than window 2.

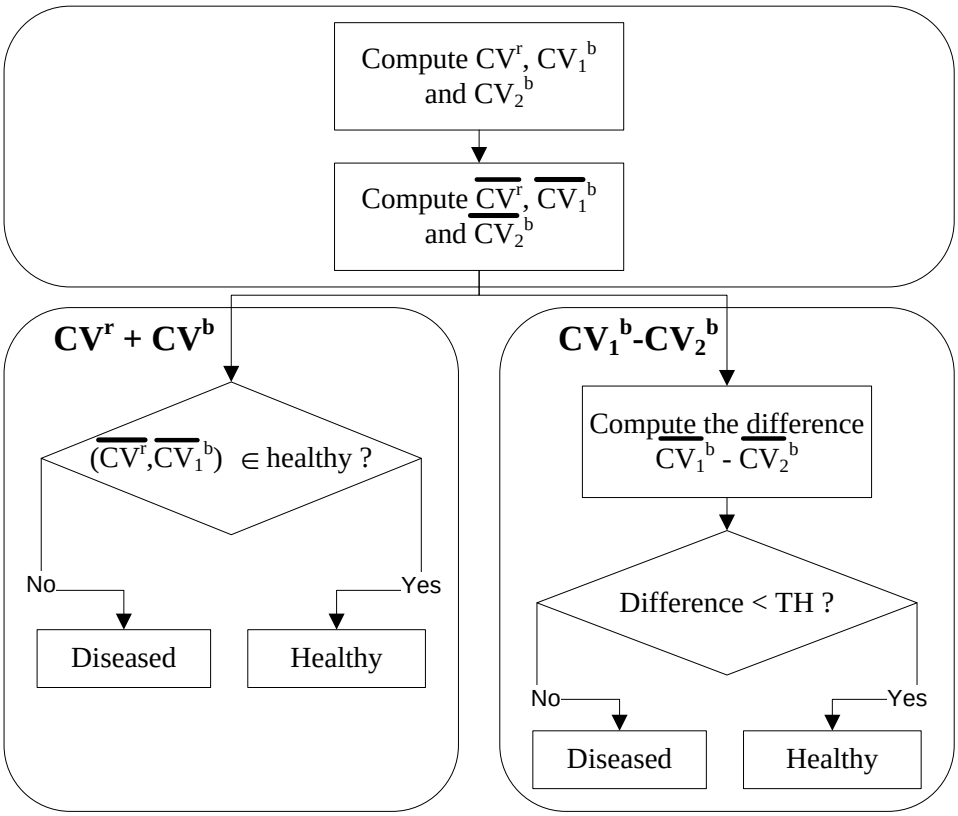

Figure 4.2. CV-based TSWV detection algorithms. TH- healthy threshold (Schor et al., submitted a).

4.2. Experiment

4.2.1. Database construction

Plants of sweet pepper (*Hazera Genetics*) were obtained from a commercial nursery (Hishtil, Ashkelon, Israel) 40-50 days after seeding. The plants were transplanted into 36 pots containing soil and potting medium and were fertigated proportionally with drippers 2-3 times per day with 5:3:8 NPK fertilizer (nitrogen (N), phosphorus (P) and potassium (K)), allowing for 25-50% drainage. Irrigation water was planned to have total N, P and K concentrations of 120, 30 and 150 mg L^{-1}, respectively; electrical conductivity of water (EC) was 2.2 dS/m. Plants were maintained at 20ºC to 30ºC in a pest and disease free greenhouse where their healthy status was ascertained visually by a plant pathologists.

For comparison of NIR-R-G and RGB technologies, images were acquired in the greenhouse with two cameras; an RGB camera (PowerShot SX210 IS, Canon, USA) with a resolution of 4320x3240 pixels, and a NIR-R-G camera (ADC Lite, 520-920 nm, Tetracam, USA) with a resolution of 2048x1536 pixels. The 36 plants were divided into two subsets positioned in different greenhouse: 24 plants for PM detection and 12 for TSWV detection. Four months after transplant, 12 out of 24 plants from the PM subset were infected with PM. Starting at the appearance of the first symptom reported by the plant pathologists (two days after infection), images of both sides of 24 selected leaves (12 healthy and 12 diseased) each from a different plant were acquired every three days over a 17 day period. Three leaves (two healthy and one diseased) were torn unintentionally during data collection and their images were discarded. Two-weeks after transplanting, 6 out of 12 plants from the TSWV subset were infected with TSWV. Images of the top and sides of the plants were taken daily in the greenhouse for 15 consecutive days (days 3 to 17 after infection). As the plants were very small during the data collection period, images of plants rather than leaves were taken. For both diseases, in addition to disease intensity, the images convey pigmentation due to possible interfering nutritional or physiological disorders.

After data collection established, TSWV and PM symptoms in all images were manually marked by plant pathologists. Leaves were classified as either healthy or diseased and disease severity was additionally graded as low, medium, or high. The pathologists additionally classified the condition of each leaf on every recorded day. In the PM database the pathologist used the images of both sides of the leaf for leaf classification. For the TSWV database, leaf classification was done using only the top of the plant images.

4.2.2. Computation environment

Image analysis was conducted using a computer equipped with an Intel Core i7-3632QM 2.2 GHz processor with turbo boost up to 3.2 GHz (CPU) and 8 GB RAM with Windows 8 (64-bit) operating system. The detection algorithms were implemented using Matlab R2013b (Mathworks, USA) and statistical analysis was conducted using IBM SPSS statistics 19 (IBM, USA).

4.2.3. Parameter determination

In a preliminary analysis, the distribution of raw values of the R, G, and B channels and H, S, and V of the RGB camera, and the NIR, R, and G channels of the NIR-R-G camera for both PM and TSWV did not yield a clear discrimination between healthy and diseased pixels. For both diseases PCA offered a superior discrimination. PCA was conducted for pixels from a healthy and a diseased leaves for each disease (for TSWV with leaf vain removal) and for both cameras (RGB and NIR-R-G). Classification regions, i.e., the healthy and diseased regions, were visualized using linear discriminant analysis (LDA) and quadratic discriminant analysis (QDA). Following the discriminating process, classification thresholds compared with DP (the ratio of the pixels classified as diseased with respect to all pixels in the leaf) were empirically determined using a box plot graph. Classification quality was established using 10x2 cross validation.

The average and standard deviation of CV of each channel (R, G, and B) in different window sizes (5x5 to 135x135 pixels in steps of 10) was calculated for 24 sample images (two healthy leaves and two infected leaves over six days). Based on examination of specificity values and runtime, window sizes for both algorithm

variants were chosen. Specificity reflects the ratio of infected plants which the algorithm correctly recognizes (Everitt and Skrondal, 1998):

$$specificity = \frac{TN}{TN + FP} \tag{3}$$

Where healthy is regarded as positive and diseased is regarding as negative. FP is false positive, and TN is true negative. Specificity is used rather than accuracy since for TSWV high identification rate of infected plants is critical.

For the CV_1^b-CV_2^b algorithm, the decision threshold was empirically determined using a box plot graph while for the CV^r +CV^b algorithm, the region of the healthy class was determined using LDA and QDA. For both algorithms classification quality was established using 10x2 cross validation.

4.2.4. Analysis

Results are presented using confusion matrixes along with overall accuracy which reflects the ratio of correct classifications (both healthy and diseased):

$$accuracy = \frac{TP + TN}{TP + FP + FN + FN} \tag{4}$$

Where TP is true positive and FN is false negative.

4.3. Results

4.3.1. TSWV detection

A total of 72 RGB images and 72 NIR-R-G images were analyzed from the TSWV database: 36 images of healthy and 36 images of infected plants. A total of six images were excluded from each RGB and NIR-R-G database; images of three infected plants taken 12 days after infection because visible symptoms had not yet appeared, and three images taken 14, 15 or 16 days after infection due to the

pathologist detection errors. The visible symptoms of TSWV appear about 12 days after infection and at the 17th day the symptoms are usually clearly visible. Accordingly, analyzed images of infected plants were taken from plants with leaves marked as having low and medium severity of TSWV (18 low, 12 medium) 12 to 17 days after infection. Analyzed images of healthy leaves were taken from day-matched leaves. Additionally, TSWV symptoms usually appear at the top of the plant, therefore all analyzed images were taken from the top view. Visual inspection by a plant pathologist verified that TSWV symptoms were indeed undetectable from the side view.

PCA-based pixel classification of RGB images achieved accuracy of 85.6% and 83.5% using QDA and LDA respectively. Therefore, QDA was selected (Fig. 4.3). The healthy threshold (TH) was determined to 0.34 (using a box plot graph) and leaf classification accuracy was 90%. Detailed results of PCA-based pixels classification are in Appendix I-1.

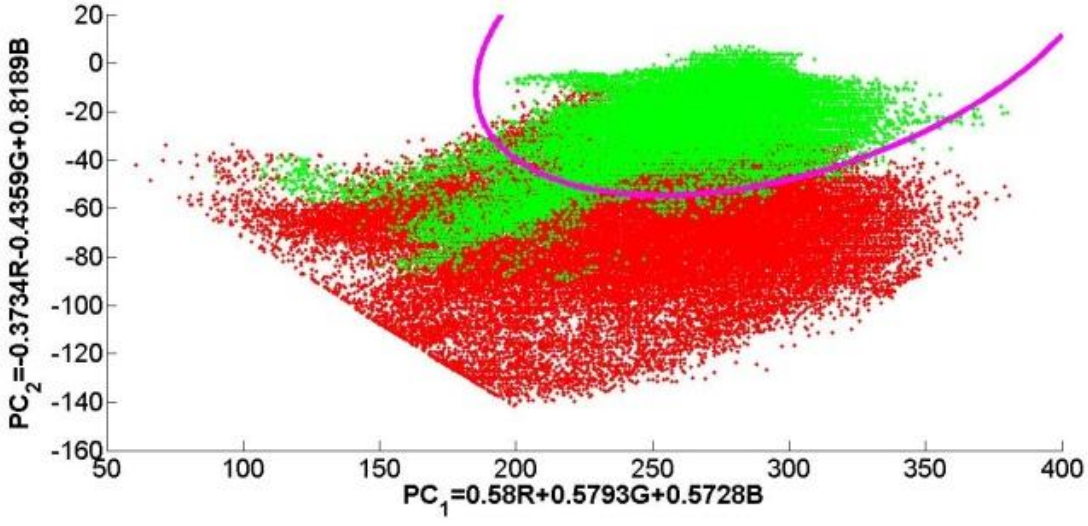

Figure 4.3. First (PC1) versus second (PC2) principal components of R, G and B variables for TSWV infected and healthy pepper plants. Altogether 60000 healthy (green) and 60000 diseased (red) pixels are displayed. The pink solid line represents the functions separating the decision regions (Schor et al., submitted b).

Visual examination of PCA-based pixel classification of NIR-R-G images (Fig. 4.4) shows that the cluster of healthy pixels is contained within the cluster of diseased pixels making NIR-R-G based classification inferior from RGB based classification. PCA-based pixel classification of NIR-R-G images achieved accuracy of 60.0% and 61.1% using QDA and LDA respectively.

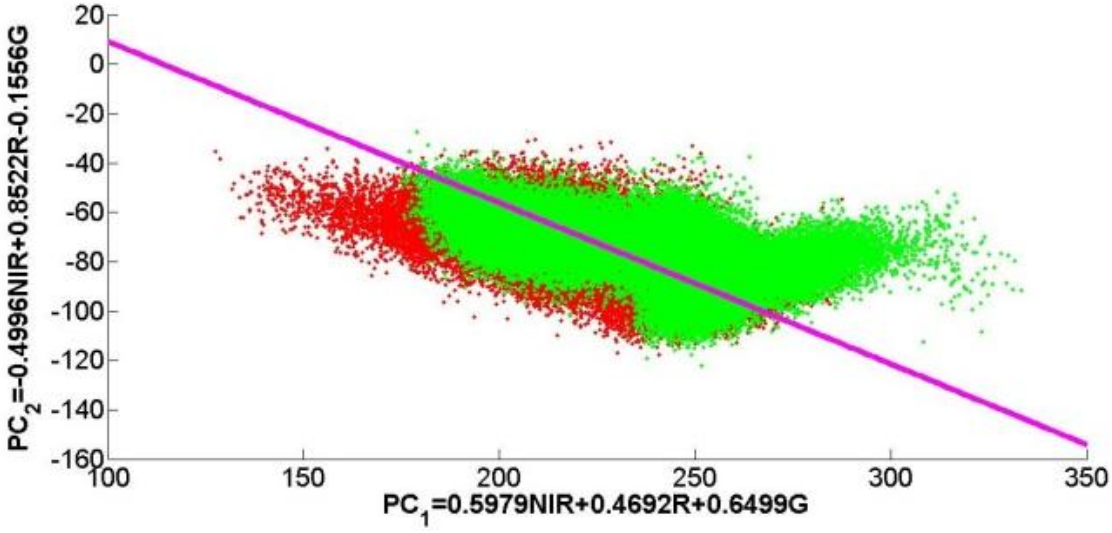

Figure 4.4. First (PC1) versus second (PC2) principal components of NIR, R, and G variables for TSWV infected and healthy pepper plants. Altogether 60000 healthy (green) and 60000 diseased (red) pixels are displayed. The pink solid line represents the functions separating the decision regions (Schor et al., submitted b).

For average CV calculation, smaller windows incurred shorter run times while larger windows had better specificity, nevertheless run time increased rapidly with window size than specificity. For example, for image of 288x352 pixels, a 35x35 window size average run time for a sample of four leaves was 19 sec while the specificity was 80%. For a 125x125 window size the average run time was 32 sec and specificity was 83% (Appendix I-2). Therefore, a window size of 35x35 was chosen for CV^r+CV^b classification. For this algorithm QDA outperformed LDA obtaining accuracy of 84%. An example of the decision region is shown in Fig. 4.5.

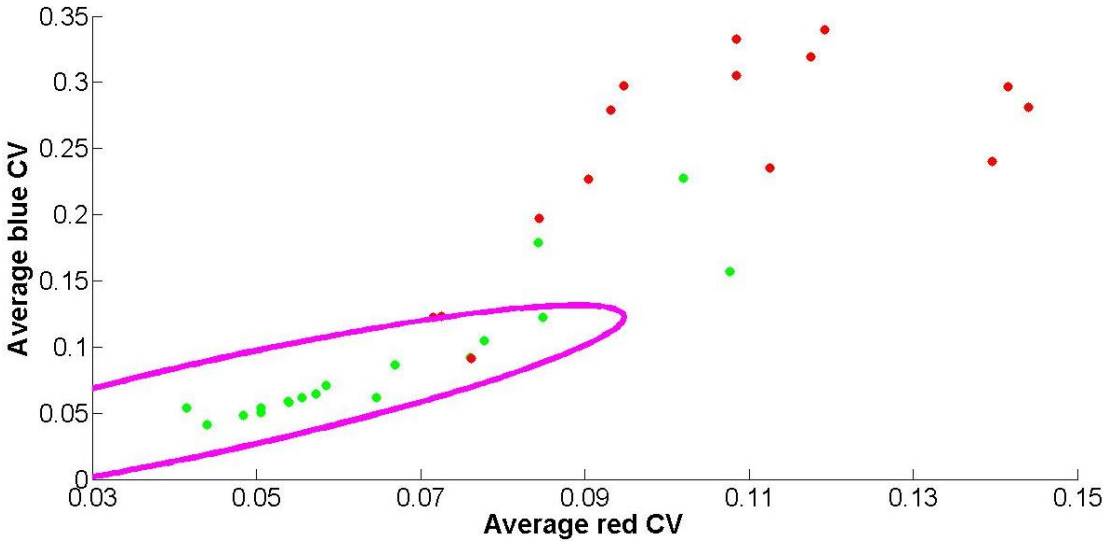

Figure 4.5. Distributions of average red CV and average blue CV values of TSWV 35x35 window size: green- healthy; red- diseased. The pink solid line represents the QDA function separating the decision regions (Schor et al., submitted a).

Fig. 4.6 shows that with increase in window size, $\overline{CV^b}$ values increase in diseased leaves more than in healthy leaves especially in the 5x5 to 65x65 window sizes.

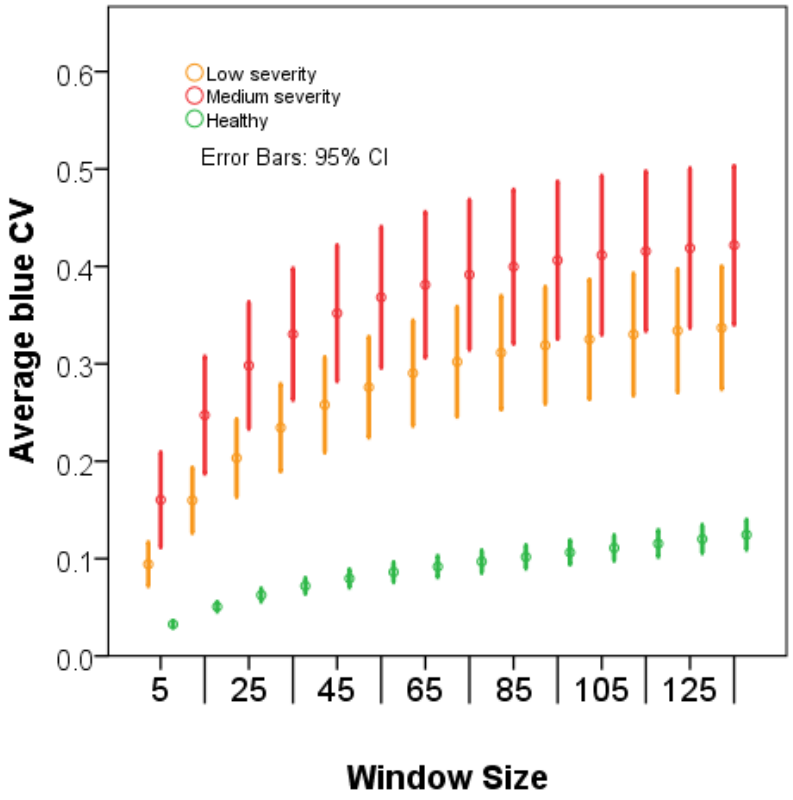

Figure 4.6. $\overline{CV^b}$ distribution in different window sizes for 12 images of healthy leaves and 12 images of infected leaves. Error bars stand for 95% confidence interval (CI) (Schor et al., submitted a).

Window sizes of 55x55, 25x25 and 15x15 were compared for large window (5x5 was the small window in all comparisons), while window size of 25x25 obtained the highest accuracy. Therefore, CV_1^b-CV_2^b classification was conducted with window sizes of 25x25 (large window) and 5x5 (small window). The healthy threshold (TH) was determined to 0.0493 (using a box plot graph) and the accuracy was 87%.

The average confusion matrix of leaf condition classification for all algorithms based on RGB images are presented in Table 4.1. Cross-validation detailed results of RGB leaf condition classification are in Appendix I-3.

Table 4.1. Leaf condition classification confusion matrix - RGB images of TSWV 12 to 17 days after infection (Schor et al., submitted a)

			Actual	
			Healthy mean (STD)	*Diseased mean (STD)*
Predicted	**PCA-based**	*Healthy*	89.4% (6.7%)	9.3% (5.6%)
		Diseased	10.6% (6.7%)	90.7% (5.6%)
	CV^r+ CV^b window size 35x35	*Healthy*	91.1% (5.4%)	24.0% (11.8%)
		Diseased	8.9% (5.4%)	76.0% (11.8%)
	CV_1^b-CV_2^b window sizes 25x25 and 5x5	*Healthy*	85.0% (5.3%)	10.0% (5.7%)
		Diseased	15.0% (5.3%)	90.0% (5.7%)
Number of leaves			18.0	15.0

4.3.2. PM detection

A total of 45 RGB images and 45 NIR-R-G images were analyzed from the PM database: 15 images of healthy leaves and 30 images of infected leaves. Analyzed images of infected plants were taken from plants with leaves marked as having low and medium severity of PM (11 low, 19 medium) of the upper side of the leaf which

is naturally visible and from which the robotic system is planned to acquire images for PM detection.

PCA-based pixel classification of RGB images achieved accuracy of 95.2% and 94.8% using QDA and LDA, respectively. Therefore, QDA was selected (Fig. 4.7). The healthy threshold (TH) was determined to 0.08 and the severity threshold (TS) was determined to 0.2. Both thresholds (TH and TS) were determined using a box plot graph. Leaf classification accuracy was 64.3%.

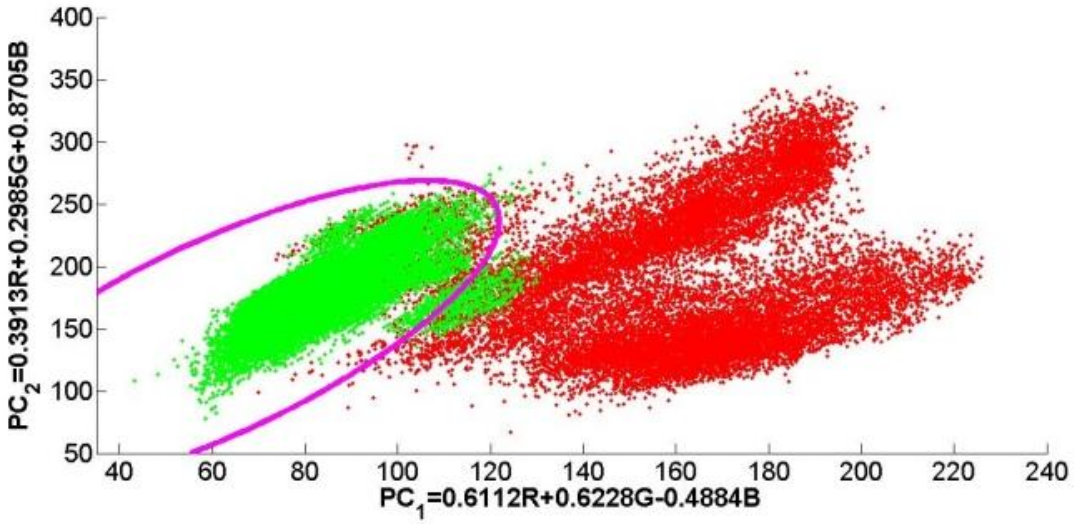

Figure 4.7. First (PC1) versus second (PC2) principal components of R, G and B variables for PM infected and healthy pepper plants. Altogether 20000 healthy (green) and 20000 diseased (red) pixels are displayed. The pink solid line represents the functions separating the decision regions (Schor et al., submitted b).

The average confusion matrix of leaf condition classification based on RGB images is presented in Table 4.2. Cross-validation detailed results of RGB leaf condition classification are in Appendix II-1.

Visual examination of PCA-based pixel classification of NIR-R-G images (Fig. 4.8) shows that the cluster of healthy pixels is contained within the cluster of diseased pixels making NIR-R-G based classification inferior from RGB based classification. PCA-based pixel classification of NIR-R-G images achieved accuracy of 71.6% and 79.9% using QDA and LDA respectively.

Table 4.2. Leaf condition classification confusion matrix - RGB images of PM (Schor et al., submitted a)

		Actual		
		Healthy mean (STD)	*Low severity mean (STD)*	*Medium severity mean (STD)*
Predicted	*Healthy*	71.2% (18.0%)	35.8% (10.7%)	15.5% (5.4%)
	Low severity	27.4% (17.1%)	45.3% (18.2%)	8.2% (8.1%)
	Medium severity	1.4% (4.3%)	18.9% (15.4%)	76.3% (11.1%)
Number of leaves		7.3	5.3	9.7

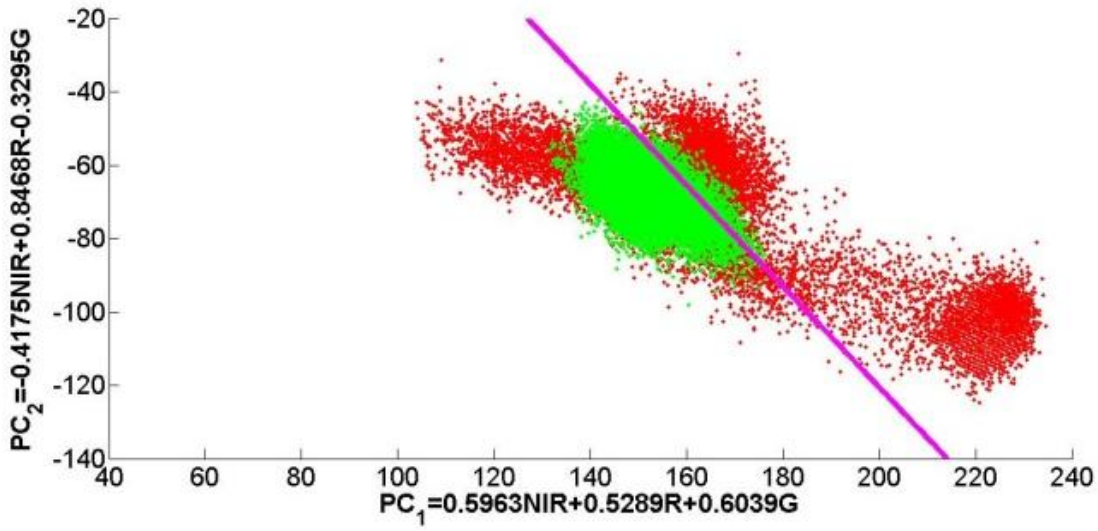

Figure 4.8. First (PC1) versus second (PC2) principal components of NIR, R, and G variables for PM infected and healthy pepper plants. Altogether 20000 healthy (green) and 20000 diseased (red) pixels are displayed. The pink solid line represents the functions separating the decision regions (Schor et al., submitted b).

The spectral indices for multispectral NIR-R-G sensor suggested by Oberti et al. (2014) for PM detection in grapevine were examined for a sample of healthy and infected pixels in bell pepper plants (Fig. 4.9). A separation accuracy of 59.0% and 66.3% using QDA and LDA respectively was attained.

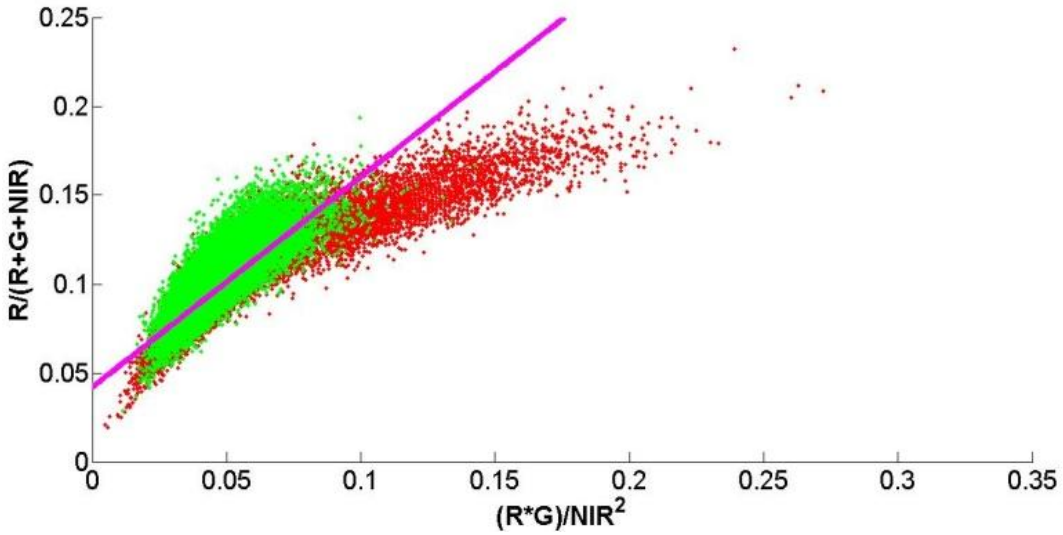

Figure 4.9. First index ($R*G/NIR^2$) versus second index (R/(R+G+NIR)) of NIR, R, and G variables for PM infected and healthy pepper plants. Altogether 20000 healthy (green) and 20000 diseased (red) pixels are displayed. The pink solid line represents the functions separating the decision regions (Schor et al., submitted b).

4.4. Discussion

For TSWV RGB-based detection, highest accuracy was obtained for PCA-based classification algorithm (90%), yet CV-based classification was also high ($CV^r+CV^{b:}$ 84% and CV_1^b-CV_2^b: 87%). Since PCA-based method may be susceptible to changing light conditions in the field, thus CV-based methods will be further examined. These results ascertain that TSWV can indeed be identified by images taken from above the plant and detect the disease 12-17 days from infection. Results additionally showed that TSWV cannot be identified from images taken from the side of the plant and thus two detection poses are required for a system identifying both diseases (PM from the side and TSWV from above) as anticipated. For the CV-based methods, correct identification of healthy leaves is high for the CV^r+CV^b method (91%) while correct identification of infected leaves is high for the CV_1^b-CV_2^b method (90%). Therefore integration of these two methods may lead to higher detection accuracy.

High accuracy was obtained for RGB images of PM at the pixels level (95%) using PCA-based classification. However, while correct detection of leaves with medium severity (76%) or healthy leaves (71%) was high, correct detection of leaves with low severity was very low (45%) making the overall classification accuracy of leaf condition low (64%). This is caused since PM symptoms start appearing on the bottom side of the leaf while the analyzed images were taken from the top of the leaf which is naturally visible. The results clearly demonstrate that for early detection, the bottom side of the leaf must be inspected. Thus a subsystem facilitating exposure of the underside of the leaf, e.g., an air blower along with a fast camera is required.

For both diseases, TSWV and PM, NIR-R-G PCA-based classification was inferior to RGB PCA-based classification, since in the NIR-R-G imagery the region of healthy pixels is contained in the region of diseased pixels. For PM, previous classification based on the NIR-R-G indices was developed for grapevine (Oberti et al., 2014). Our results ascertain that PM has different symptoms and different progression characteristics (color, pattern, growth region, etc.) in different cultivars, e.g., grapevine and bell peppers. This is in line with additional finding that specific detection procedures are required for each disease and cultivar.

5. Preliminary prototype integration

5.1. General

The prototype integration tests examined compatibility of system components (mechanical structure, sensor suite, motion planning, and detection algorithms) and system integrated performance. The examination of the developed diseases detection algorithms (section 4.3) clearly demonstrated that the NIR-R-G camera did not achieve improved detection accuracy over the RGB camera, therefore the NIR-R-G camera was turned off during the experiment and only the RGB camera was used for disease detection.

Different plant locations with respect to the robotic system base were tested in order to examine suitability of required motion profiles and the robotic workspace. Different end-effector velocities were tested for ascertaining manipulator precision capabilities and the accuracy of the laser sensor.

5.2. Computation environment

The detection system was controlled and operated by a computer equipped with an Intel Pentium Dual E2180 2 GHz processor (CPU) and 2 GB RAM with Windows XP (32-bit) operating system. The detection process and detection algorithms were implemented using Matlab R2009b (Mathworks, USA).

5.3. Protocol

The experiment was conducted in the laboratory and was done under nine combinations of two independent variables: three end-effector velocities (5, 15 and 25 mm/sec) and three different plant locations (770, 900 and 1050 mm away from the robotic system base in workspace coordinate). Each condition was repeated with 10 healthy plants. The plants were positioned on a conveyor belt with black

background for simplifying plant identification and background removal (Fig. 5.1). The conveyor was not moving during the detection process, so the plant was static.

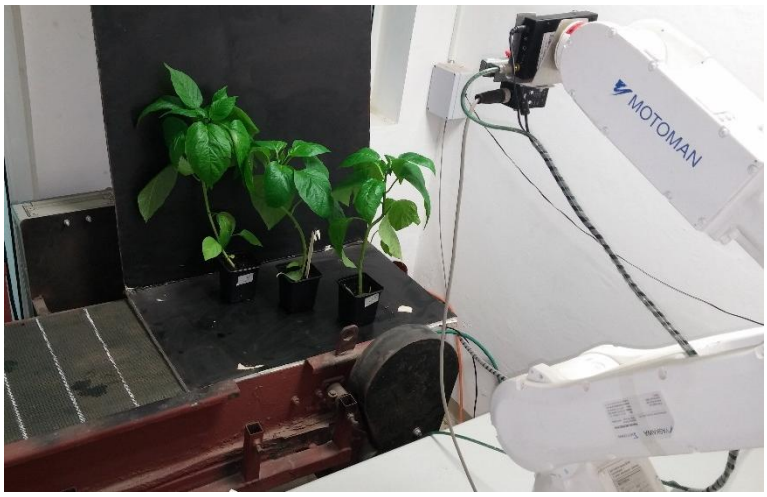

Figure 5.1. Experiment apparatus

5.4. Analysis

Possible collisions were visually observed during the test. It is critical to avoid collisions in this application since plant destruction along with passing the diseases from one plant to another as result of contact with plants must be prevented.

Execution time (sec) was computed for each sub-task to determine the most time consuming sub-task. Cycle time (sec) was determined as the sum of all sub-tasks: position manipulator above the plant, plant location and TSWV pose determination, TSWV detection, manipulator movement to intermediate-point, position manipulator alongside the plant, plant location and PM pose determination, PM detection, and manipulator movement to next plant.

In addition, two measures were used to quantify performance of the supporting vision analysis:

- Plant identification success (%): the number of plants correctly identified as plants divided by the total number of plants. This indicator provides a measure for the quality of the plant location algorithm.

- Correct camera positioning success (%): the number of correct positioning of the camera divided by the number of correctly identified plants. Correct positioning (Fig. 5.2) is determined when the center of the image is situated inside the plant center area box defined in section 3.2. This indicator was added to assess the motion execution quality of the manipulator and the camera pose determination algorithm. Incorrect camera positioning can originate from imperfect numerical iterative search (computation issue) or from incomplete implementation of the inverse kinematic solution (motion control issue).

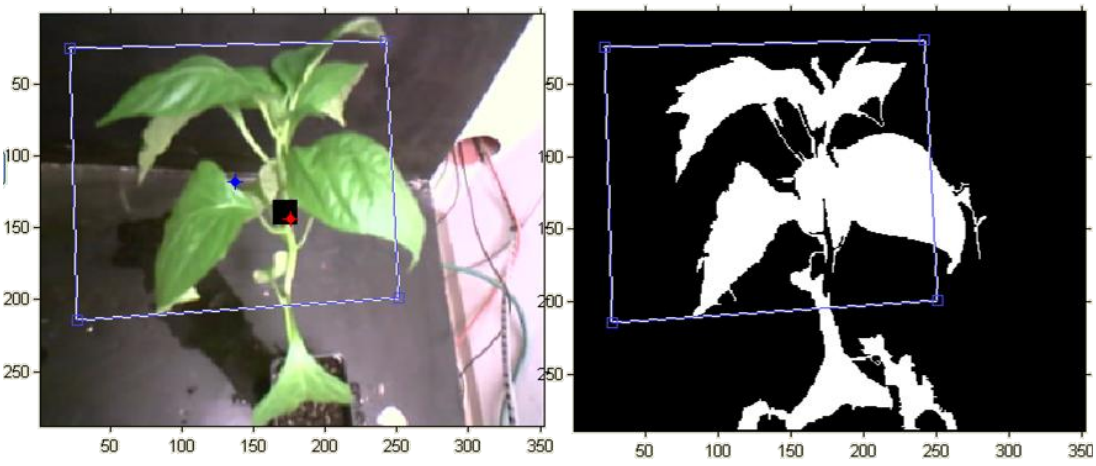

Figure 5.2. Correct positioning of the camera (left), i.e. the center of the image (red dot) is situated inside the plant center area box (black box). Binary image of the plant (right). Further details about the notations in Appendix III-1.

5.5. Results

Collisions were observed only for plants located 770 mm from the robotic system base. A total of five collisions were observed over 30 repetitions (10 plants and three end-effector velocities). Two collisions occurred when the manipulator moved from

the TSWV detection pose to the intermediate-point, and three collisions occurred when the manipulator moved from the intermediate-point to the PM detection pose.

The integrated system operated for 110 consecutive minutes where 10 healthy plants were analyzed under nine conditions (total of 90 repetitions). Fig. 5.3 presents the average execution time per sub-task. Detailed results of the execution time pre sub-task are described in Appendix III-2. As shown, plant location and camera pose determination, for both TSWV and PM are time consuming sub-tasks. The total time (summation of sub-tasks detailed in Fig. 5.3, without diseases detection execution times that depends on the algorithm type) was 42.8, 26.5 and 24.2 second for end-effector velocity of 5, 15 and 25 mm/sec, respectively.

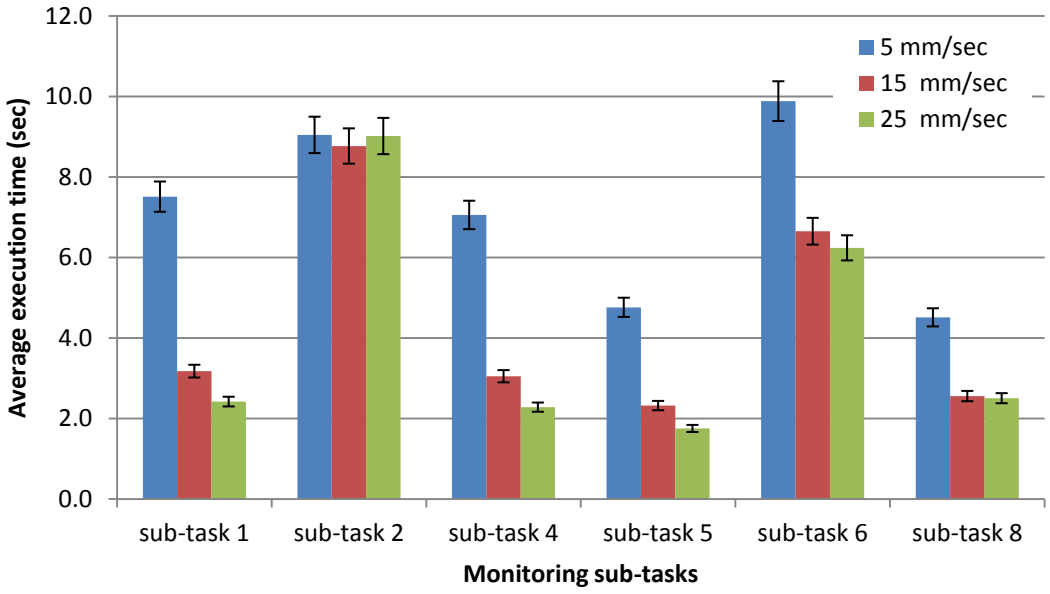

Figure 5.3. Average execution time per sub-task. 1-position manipulator above the plant; 2-plant location and TSWV pose determination; 4-manipulator movement to intermediate-point; 5-position manipulator alongside the plant; 6-plant location and PM pose determination; 8-manipulator movement to next plant.

Average cycle times for different end-effector velocities are presented in Fig. 5.4. The shortest disease detection execution time was obtained for PCA-based

algorithms (0.06 sec). Much longer execution times were obtained for CV-based algorithms (CV^r+CV^b: 108 sec and CV_1^b-CV_2^b: 154 sec).

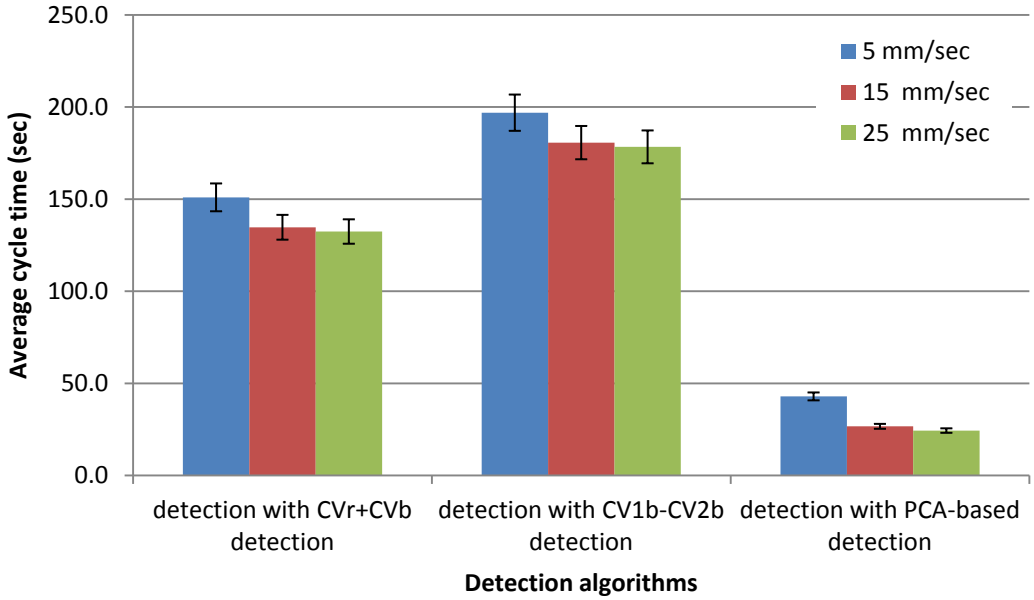

Figure 5.4. Average cycle time (including disease detection).

Fig. 5.5 presents the average results of plant identification success and correct camera positioning success. Detailed results of the performance indicators are listed in Appendix III-2. High plant identification success was obtained for PM pose (sensor apparatus alongside the plant) for all plant locations (770 mm: 90%, 900 mm: 96%, 1050 mm: 93%, average: 93%). For TSWV plant identification success (average: 83%) was high for close and medium distance plants (770 mm: 100% and 900 mm: 90%), whereas for remote plants it was low (1050 mm: 60%). A high correct camera positioning success per total identified plants was obtained for the PM pose (770 mm: 81%, 900 mm: 86%, 1050 mm: 82%, average: 83%) while for the TSWV pose the success rate was very low (770 mm: 47%, 900 mm: 33%, 1050 mm: 17%, average: 32%).

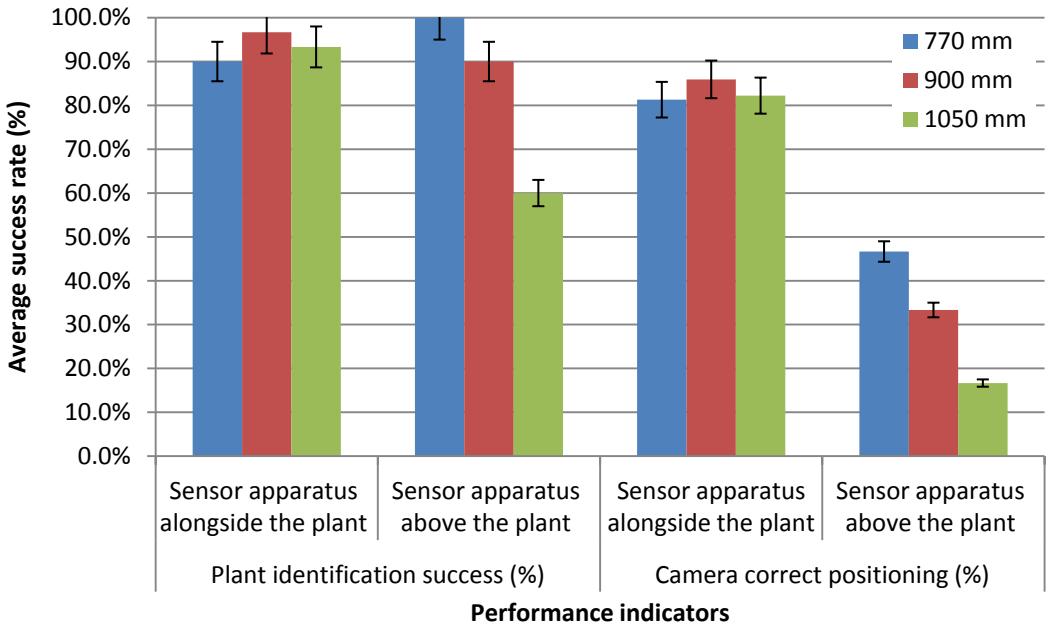

Figure 5.5. Average results of plant identification success and correct camera positioning success.

5.6. Discussion

All collisions occurred when the manipulator moved to and from the intermediate-point for close distance plants. This suggests that the intermediate-point should be redefined. Alternatively it could be dynamically adjusted according the plant distance.

CV-based detection algorithms execution time was long and formed a critical influence on cycle time (Fig. 5.4) due to the scanning process. The computer that was used for controlling the robotic system during the integration tests (section 5.2) was equipped with very low computation power. By using a more powerful state-of-the-art computer the execution time can be reduced considerably, e.g., by over 500% to 20.1 sec (CV^{r}+CV^{b}) and by over 400% to 36.4 sec ($CV_1{}^{b}$-$CV_2{}^{b}$) (section 4.2.2).

For PM, results indicate that the sensor apparatus can be positioned alongside the plant for performing detection (plant identification success of 93% and correct camera positioning success of 83%). For TSWV, results indicate that the system has

difficulty in successfully positioning the sensor apparatus above the plant for (plant identification success of 83% and correct camera positioning success of 32%). Using a longer arm or changing arm positioning with respect to the conveyer should be examined.

6. Conclusions and future work

The current research targets the development of a robotic disease detection system for greenhouse peppers. Within the course of the research was have developed the first disease detection algorithms based on visible spectral imagery of two major threats of greenhouse bell peppers suitable for analysis during a single pass of the robotic manipulator over the plant. An algorithm based on PCA was developed for detection of PM and three algorithms were developed for detection of TSWV, one based on PCA and two on CV. For TSWV, PCA-based classification with leaf vain removal, achieved the highest classification accuracy (90%) and the accuracy of the CV methods was also high (85%, 87%). For PM, pixel-level classification was high (95.2%) while leaf condition classification accuracy was low (64.3%) since it was determined based on the top side of the leaf while disease symptoms start appearing on its bottom side.

Preliminary prototype integration was conducted with a complete operation average cycle time of 26.7 sec (with PCA-based detection), 134.7 sec (with CV^r+CV^b detection) and 180.7 sec (with CV_1^b-CV_2^b detection) for end-effector velocity of 15 mm/sec. The results of the preliminary integration tests show that the sensor apparatus can be properly positioned alongside the plant for PM detection (correct camera positioning success of 83% per total identified plants). However, the results also demonstrate difficulty in successfully positioning the sensor apparatus above the plant for TSWV detection (correct camera positioning success of 32% per total identified plants).

Future research will examine improvement of the disease detection algorithms aiming to achieve higher accuracy along with earlier detection, e.g., by facilitating

PM examination in the bottom side of the leaf, by integration of the two CV-based methods or by choosing different detection algorithm in different conditions. For complete integration tests and field performance studies, a leaf segmentation algorithm, and a dynamic detection process (i.e., the conveyor carrying pepper pots moving during the detection process) will be implemented.

Appendix I. Detailed results of TSWV detection

I-1. PCA-based pixel classification

PCA-based pixel classification was conducted on separated days in order to evaluate TSWV progress. Fig. I.1 represents the distributions of PCA values of TSWV for healthy and diseased pixels at different days after infection.

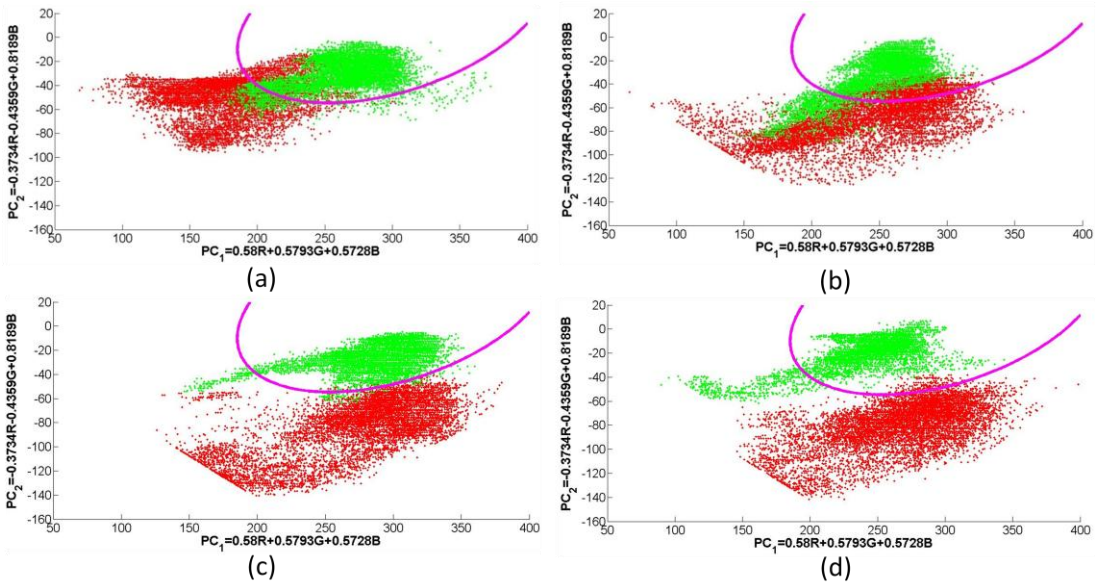

Figure I.1. First (PC1) versus second (PC2) principal components of R, G and B variables for TSWV infected and healthy pepper plants at 12, 14, 16 and 17 days after infection (sub graphs a-d respectively). At each sub graph 10000 healthy (green) and 10000 diseased (red) pixels are displayed. The pink solid lines represent the functions separating the decision regions.

Fig. I.1 shows that while the position of the cluster of healthy areas remained unchanged with time (means: (265,-29), (252,-29), (288,-27), (248,-18) and standard deviation: (27,11), (24,15), (27,10), (26,10) for 12, 14, 16 and 17 days after infection, respectively), the distribution of diseased area gradually shifted and expanded towards high values of PC1 and low values of PC2 (means: (182,-49), (244,-67), (278,-79), (272,-76) and standard deviation: (33,15), (45,19), (44,21), (37,17) for 12, 14, 16 and 17 days after infection, respectively). The average classification confusion matrixes for PCA-based pixel classification for different

days after infection are presented in Table I.1. Those results clearly demonstrates that the separation among healthy and diseased pixels increased noticeably with time making TSWV detectable

Table I.1. Confusion matrix for PCA-based pixel classification for different days after infection - TSWV

			Actual	
			Healthy	*Diseased*
Predicted	**12 days after infection**	*Healthy*	92.7%	18.8%
		Diseased	7.3%	81.2%
	14 days after infection	*Healthy*	88.0%	25.8%
		Diseased	12.0%	74.2%
	16 days after infection	*Healthy*	96.9%	0.7%
		Diseased	3.1%	99.3%
	17 days after infection	*Healthy*	94.1%	3.0%
		Diseased	5.9%	97.0%

I-2. CV^r+CV^b classification in different window sizes

For average CV calculation, smaller windows incurred shorter run times (Fig. I.2) while larger windows had better specificity (35x35 window size specificity is 80%; 75x75 window size specificity is 82%; and 125x125 window size specificity is 83%). Nevertheless, run time increased rapidly with window size than specificity, therefore, a window size of 35x35 was chosen for CV^r+CV^b classification (Fig. 4.5). For comparison, Fig. I.3 presents an example of the decision region for a 125x125 window size with QDA.

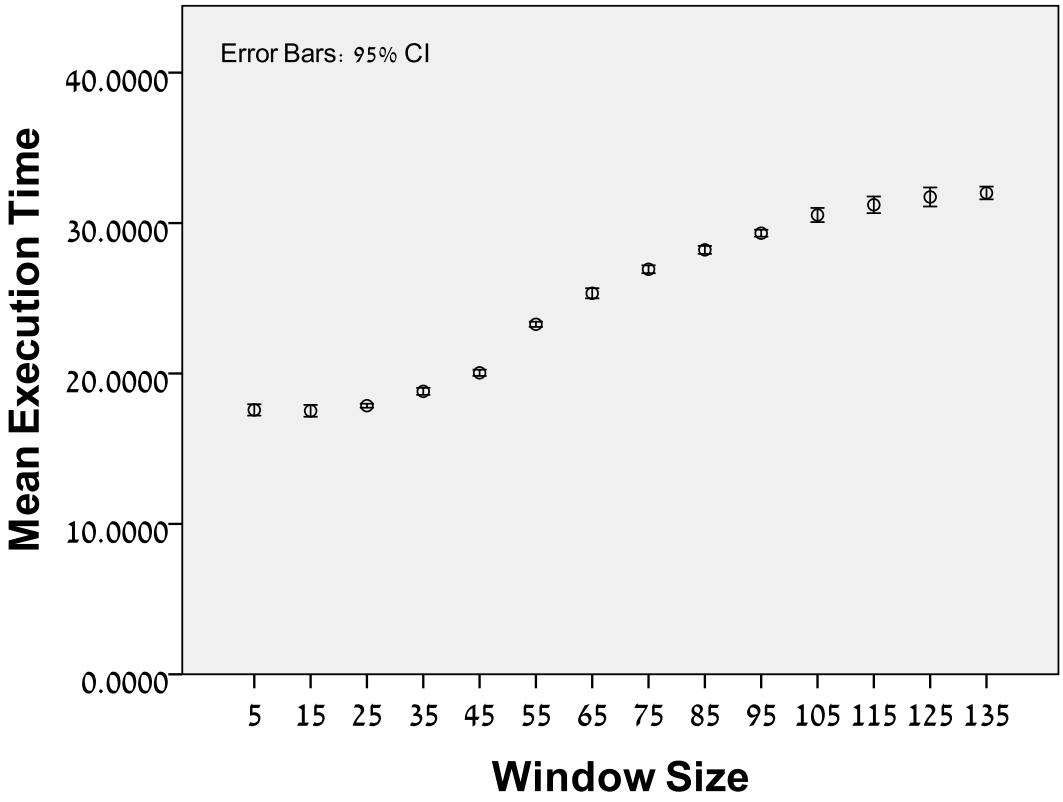

Figure I.2. Distribution of CV^r+CV^b classification algorithm execution time in different window sizes for four images (images size is 288x352 pixels). Error bars stand for 95% confidence interval (CI).

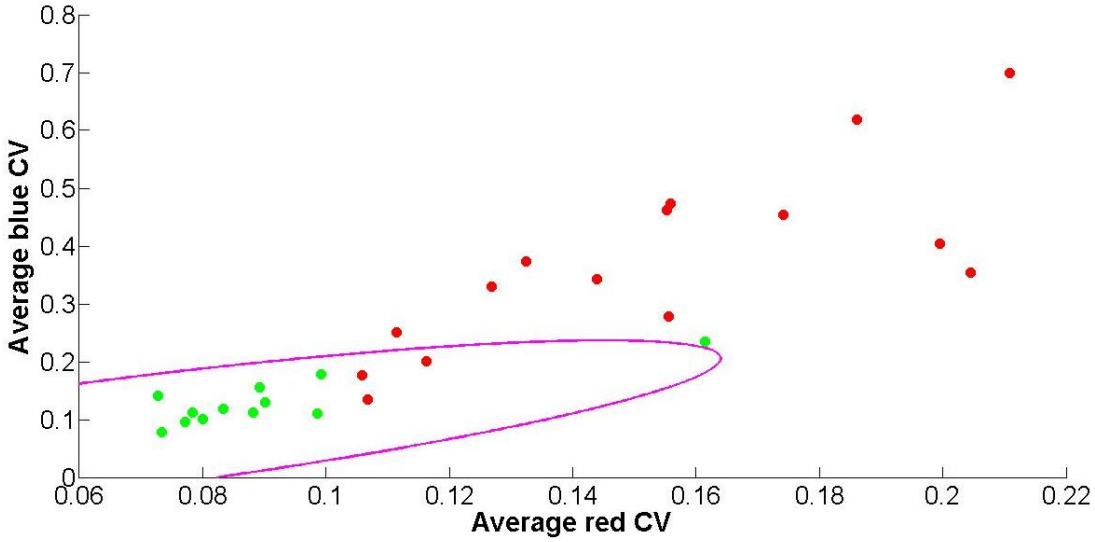

Figure I.3. Distributions of average red CV and average blue CV values of TSWV 125x125 window size: green- healthy; red- diseased. The pink solid line represents the QDA function separating the decision regions.

I-3. Leaf condition classification 10x2 cross-validation

All the developed classification algorithms qualities were established using 10x2 cross validation. As described at section 4.3.1, a total of 36 images of healthy and 30 images of infected plants (six images were excluded) were analyzed from the TSWV database. The cross-validation detailed results are presented in Table I.2.

Table I.2. Leaf condition classification cross-validation - RGB images of TSWV 12 to 17 days after infection

		TP ***mean (STD)***	***FP*** ***mean (STD)***	***FN*** ***mean (STD)***	***TN*** ***mean (STD)***
PCA-based	1	77.8%	6.7%	22.2%	93.3%
	2	83.3%	6.7%	16.7%	93.3%
	3	94.4%	13.3%	5.6%	86.7%
	4	88.9%	6.7%	11.1%	93.3%
	5	100.0%	6.7%	0.0%	93.3%
	6	94.4%	20.0%	5.6%	80.0%
	7	94.4%	13.3%	5.6%	86.7%
	8	83.3%	13.3%	16.7%	86.7%
	9	88.9%	6.7%	11.1%	93.3%
	10	88.9%	0.0%	11.1%	100.0%
	total	89.4% (6.7%)	9.3% (5.6%)	10.6% (6.7%)	90.7% (5.6%)
CV^r+ CV^b window size 35x35	1	83.3%	6.7%	16.7%	93.3%
	2	88.9%	33.3%	11.1%	66.7%
	3	83.3%	20.0%	16.7%	80.0%
	4	94.4%	13.3%	5.6%	86.7%
	5	88.9%	20.0%	11.1%	80.0%
	6	94.4%	40.0%	5.6%	60.0%
	7	94.4%	20.0%	5.6%	80.0%

	8	88.9%	13.3%	11.1%	86.7%
	9	94.4%	33.3%	5.6%	66.7%
	10	100.0%	40.0%	0.0%	60.0%
	total	91.1% (5.4%)	24.0% (11.8%)	8.9% (5.4%)	76.0% (11.8%)
CV_1^b-CV_2^b window sizes 25x25 and 5x5	1	77.8%	6.7%	22.2%	93.3%
	2	83.3%	13.3%	16.7%	86.7%
	3	88.9%	13.3%	11.1%	86.7%
	4	77.8%	6.7%	22.2%	93.3%
	5	88.9%	0.0%	11.1%	100.0%
	6	83.3%	13.3%	16.7%	86.7%
	7	94.4%	13.3%	5.6%	86.7%
	8	83.3%	6.7%	16.7%	93.3%
	9	88.9%	20.0%	11.1%	80.0%
	10	83.3%	6.7%	16.7%	93.3%
	total	85.0% (5.3%)	10.0% (5.7%)	15.0% (5.3%)	90.0% (5.7%)

Appendix II. Detailed results of PM detection

II-1. Leaf condition classification 10x2 cross-validation

PCA-based developed classification algorithm quality was established using 10x2 cross validation. As described at section 4.3.2, a total of 45 images were analyzed from the PM data base: 15 images of healthy leaves, 11 images of leaves with low severity symptoms and 19 images of leaves with medium severity. The cross-validation detailed results are presented in Table II.1.

Table II.1. Leaf condition classification cross-validation - RGB images of PM

			Actual		
			Healthy mean (STD)	*Low severity mean (STD)*	*Medium severity mean (STD)*
Predicted	1	*Healthy*	75.0%	16.7%	11.1%
		Low severity	25.0%	50.0%	0.0%
		Medium severity	0.0%	33.3%	88.9%
		Number of leaves	8.00	6.00	9.00
	2	*Healthy*	75.0%	40.0%	10.0%
		Low severity	25.0%	20.0%	0.0%
		Medium severity	0.0%	40.0%	90.0%
		Number of leaves	8.00	5.00	10.00
	3	*Healthy*	62.5%	40.0%	20.0%
		Low severity	37.5%	60.0%	20.0%
		Medium severity	0.0%	0.0%	60.0%
		Number of leaves	8.00	5.00	10.00
	4	*Healthy*	100.0%	40.0%	10.0%
		Low severity	0.0%	60.0%	0.0%
		Medium severity	0.0%	0.0%	90.0%
		Number of leaves	7.00	5.00	10.00

	5	*Healthy*	42.9%	20.0%	10.0%
		Low severity	57.1%	80.0%	20.0%
		Medium severity	0.0%	0.0%	70.0%
		Number of leaves	7.00	5.00	10.00
	6	*Healthy*	71.4%	33.3%	22.2%
		Low severity	28.6%	50.0%	11.1%
		Medium severity	0.0%	16.7%	66.7%
		Number of leaves	7.0	6.0	9.0
	7	*Healthy*	57.1%	40.0%	20.0%
		Low severity	42.9%	40.0%	10.0%
		Medium severity	0.0%	20.0%	70.0%
		Number of leaves	7.0	5.0	10.0
	8	*Healthy*	57.1%	50.0%	11.1%
		Low severity	28.6%	33.3%	11.1%
		Medium severity	14.3%	16.7%	77.8%
		Number of leaves	7.0	6.0	9.0
	9	*Healthy*	71.4%	40.0%	20.0%
		Low severity	28.6%	20.0%	10.0%
		Medium severity	0.0%	40.0%	70.0%
		Number of leaves	7.0	5.0	10.0
	10	*Healthy*	100.0%	40.0%	20.0%
		Low severity	0.0%	40.0%	0.0%
		Medium severity	0.0%	20.0%	80.0%
		Number of leaves	7.0	5.0	10.0
	total	*Healthy*	71.2% (18.0%)	35.8% (10.7%)	15.5% (5.4%)
		Low severity	27.4% (17.1%)	45.3% (18.2%)	8.2% (8.1%)
		Medium severity	1.4% (4.3%)	18.9% (15.4%)	76.3% (11.1%)
		Number of leaves	7.3	5.3	9.7

Appendix III. Detailed results of preliminary prototype integration

III-1. User interface

For controlling the detection system and to be able to observe the detection process from a remote location a GUI was developed (Fig. III.1). The GUI buttons control the system while the sensors output displayed in the two screens. The buttons actions are; sending the manipulator to its home position (Homing), initialize required parameters (Initialize), execute detection of only TSWV (TSWV Detection), execute detection of only PM (PM Detection), execute full detection process (Auto Monitoring) and exit the GUI (Exit). The right screen display a video of the motion as accumulates from the RGB camera and the image process conducted on the RGB images acquired. The left screen display the RGB images that acquired along with the plant center area and the center of the images of both cameras (red dot of RGB camera and blue dot of NIR-R-G camera). The blue rectangle on both screens represents the image frame of the NIR-R-G camera. The distance absorbed from the laser sensor is written below the left screen.

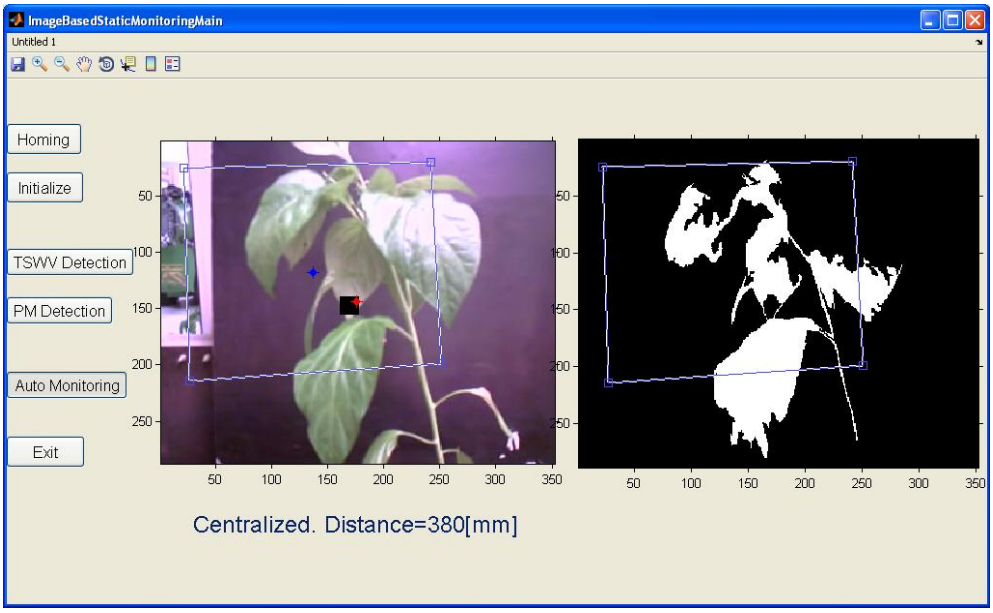

Figure III.1. Detection system GUI

III-2. Performance indicators and execution times

Table III.1 presents the performance indicator listed in section 5.4 for each of the nine combinations tested.

Table III.1. Performance indicators

End-effector velocity [mm\sec] **Plant position regarding detection system base [mm]**	**5** **770**	**5** **900**	**5** **1050**	**15** **770**	**15** **900**	**15** **1050**	**25** **770**	**25** **900**	**25** **1050**
Plant identification success (%)									
Sensor apparatus above the plant	100	90	60	100	90	60	100	90	60
Sensor apparatus alongside the plant	100	90	90	80	100	100	90	100	90
Correct camera positioning (%)									
Sensor apparatus above the plant	50	44	17	50	33	17	40	22	17
Sensor apparatus alongside the plant	80	78	67	75	90	80	89	90	100
Plant collision rate (%)	10	0	0	20	0	0	20	0	0

Table III.2 shows the mean and STD of execution times of each sub-task as defined in section 3.2 and presents the total time of sub-tasks.

Table III.2. Mean (STD) of execution time per sub-task [sec]

End-effector velocity [mm\sec] **Plant position regarding detection system base [mm]**	**5** **770**	**5** **900**	**5** **1050**	**15** **770**	**15** **900**	**15** **1050**	**25** **770**	**25** **900**	**25** **1050**
1. Position manipulator above the plant	7.5 (0.1)	7.5 (0.1)	7.5 (0.1)	3.2 (0.1)	3.2 (0.1)	3.2 (0.1)	2.4 (0.1)	2.4 (0.1)	2.5 (0.1)
2. Plant location and TSWV pose determination	9.3 (3.3)	8.3 (3.0)	9.6 (1.6)	7.8 (2.9)	8.8 (2.4)	9.6 (1.6)	8.3 (2.5)	9.1 (2.7)	9.6 (1.5)
3. TSWV detection (Table III.3)									
4. Move manipulator to central intermediate-point	7.2 (0.4)	7.0 (0.4)	7.0 (0.5)	3.1 (0.2)	3.0 (0.1)	3.0 (0.2)	2.3 (0.1)	2.2 (0.1)	2.3 (0.1)
5. Position manipulator alongside the plant	4.8	4.8	4.7	2.3	2.3	2.3	1.7	1.8	1.7

	(0.1)	(0.1)	(0.1)	(0.1)	(0.1)	(0.1)	(0.1)	(0.2)	(0.1)
6. Plant location and PM pose determination	8.2 (5.3)	10.5 (4.6)	10.9 (4.1)	5.1 (5.2)	6.4 (4.7)	8.5 (3.9)	6.8 (4.9)	5.0 (4.4)	6.9 (4.8)
7. PM detection (Table III.3)									
8. Move manipulator to next sampling plant	4.7 (0.4)	4.5 (0.5)	4.4 (0.9)	2.7 (0.2)	2.5 (0.3)	2.4 (0.3)	2.6 (0.2)	2.5 (0.2)	2.5 (0.4)
Total time (*without diseases detection execution time)	41.5 (5.7)	42.6 (4.5)	44.2 (3.9)	24.2 (4.8)	26.2 (4.3)	29.1 (2.6)	24.1 (4.6)	23.1 (3.9)	25.5 (3.1)

Table III.3 shows the mean and STD of execution times of each disease detection algorithm as defined in section 4.1.

Table III.3. Mean (STD) of execution time per disease detection algorithm [sec]

Disease detection algorithm	**Mean (STD) execution time [sec] for image of 288x352**
TSWV detection:	
PCA-based	0.069 (0.009)
CV^r+ CV^b window size 35x35	108.1 (7.491)
CV_1^b-CV_2^b window size 25x25 and 5x5	154.1 (12.976)
PM detection:	
PCA-based	0.064 (0.005)

References

Attanayake, K.P.R.N., D.A. Glawe, K.E. Mcphee, F.M. Dugan and W. Chen, "First report of powdery mildew of chickpea (Cicer arietinum) caused by Leveillula taurica in Washington State", Online, *Plant Health Progress*, 2008.

Avila, Y., J. Stavisky, S. Hague, J. Funderburk, S. Reitz and T. Momol, "Evaluation of Frankliniella bispinosa (Thysanoptera: Thripidae) as a vector of the Tomato spotted wilt virus in pepper", *Florida Entomologist*, 89(2): 204-207, 2006.

Bac, C.W., E.J. Van Henten, J. Hemming and Y. Edan, "Harvesting Robots for High-value Crops: State-of-the-art Review and Challenges Ahead", *Journal of Field Robotics*, 31(6): 888-911, 2014.

Bac, C.W., J. Hemming and E.J. Van Henten, "Robust pixel-based classification of obstacles for robotic harvesting of sweet-pepper", *Computers and Electronics in Agriculture*, 96: 148-162, 2013.

Baeten, J., K. Donné, S. Boedrij, W. Beckers and E. Claesen, "Autonomous Fruit Picking Machine: A Robotic Apple Harvester", in Proc. *6th International Conference on Field and Service Robotics*, 2008.

Bakker, T., K. Van Asselt, J. Bontsema and E.J. Van Henten, "Robotic weeding of a maize field based on navigation data of the tractor that performed the seeding", *Agricontrol*, 3(1): 157-159, 2010.

Barbedo, A., and J. Garcia, "Digital image processing techniques for detecting, quantifying and classifying plant diseases", *SpringerPlus*, 2: 660, 2013.

Baur, J., J. Pfaff, H. Ulbrich and T. Villgrattner, "Design and development of a redundant modular multipurpose agricultural manipulator", in Proc. *IEEE/ASME International Conference on Advanced Intelligent Mechatronics (AIM)*, 823-830, 2012.

Bechar, A. "Robotics in horticultural field production", *Stewart Postharvest Review*, 6(3): 1-11, 2010.

Belanger, M.C., J.M. Roger, P. Cartolaro, A.A. Viau and V. Bellon-Maurel, "Detection of Powdery mildew in grapevine using remotely sensed UV-induced fluorescence", *International journal of Remote Sensing*, 29(6): 1707–1724, 2008.

Blasco, J., N. Aleixos, J.M. Roger, G. Rabatel and E. Molte, "AE- Automation and emerging technologies: Robotic weed control using machine vision", *Biosystems Engineering*, 83: 149-157, 2002.

Bochtis, D.D. , C.G. Sørensen and S.G. Vougioukas, "Path planning for in-field navigation-aiding of service units", *Computers and Electronics in Agriculture*, 74(1): 80-90, 2010.

Bock, C.H., G.H. Poole, P.E. Parker and T.R. Gottwald, "Plant disease severity estimated visually, by digital photography and image analysis, and by hyperspectral imaging", *Critical Reviews in Plant Science*, 29: 59–107, 2010

Brittlebank, C.C., "Tomato diseases", *Journal of Agriculture Victoria*, 7: 231-235, 1919.

Bulanon, D.M., T. Kataoka, Y. Ota and T. Hiroma, "AE-automation and emerging

technologies: a segmentation algorithm for the automatic recognition of Fuji apples at harvest", *Biosystems Engineering*, 83(4): 405-412, 2002.

Bürling, K., M. Hunsche and G. Noga, "Presymptomatic detection of powdery mildew infection in winter wheat cultivars by laser-induced fluorescence", *Applied Spectroscopy*, 66(12): 1411-1419, 2012.

Cerkauskas, R.F. and A. Buonassisi, "First report of Powdery mildew of greenhouse pepper caused by Leveillula taurica in British Columbia, Canada", *Plant Disease*, 87(9): 1151, 2003.

Crescenzi, A., A. Viggiano and A. Fanigliulo, "Resistance breaking tomato spotted wilt virus isolates on resistant pepper varieties in Italy", *Commun. Agric. Appl. Biol. Sci.*, 78(3): 609-612, 2013.

Dong, X., M.C. Vuran and S. Irmak, "Autonomous precision agriculture through integration of wireless underground sensor networks with center pivot irrigation systems", *Ad Hoc Networks*, 11(7): 1975-1987, 2013.

Dong, F., O. Petzold, W. Heinemann and R. Kasper, "Time-optimal guidance control for an agricultural robot with orientation constraints", *Computers and Electronics in Agriculture*, 99: 124-131, 2013.

Du Toit, L.J., D.A. Glawe and G.Q. Pelter, "First report of powdery mildew of onion (Allium cepa) caused by Leveillula taurica in the Pacific Northwest", Online, *Plant Health Progress*, 2004.

Edan, Y., D. Rogozin, T. Flash and G.E. Miles, "Robotic Melon Harvesting", *IEEE Transactions on Robotics and Automation*, 16(6): 831-835, 2000.

Eizicovits, D., B. Van Tuijl, S. Berman and Y. Edan, "Integration of perception capabilities in gripper design using graspability maps", *Biosystems Engineering*, submitted for publication.

Elad, Y., Y. Messika, M. Brand, D. Rav David and A. Sztejnberg, "Effect of microclimate on Leveillula taurica Powdery mildew of sweet pepper", *Phytopathology*, 97(7): 813-824, 2007.

Everitt, B.S., and A. Skrondal, *The Cambridge Dictionary of Statistics*, New York: Cambridge University Press, 1998.

Fereres, A. and B. Raccah, "Plant virus transmission by insects," *eLS*, 1-12, 2015.

Foglia, M.M. and G. Reina, "Agricultural Robot for Radicchio Harvesting", *Journal of Field Robotics*, 23(6): 363, 2006.

Franke, J. and G. Menz, "Multi-temporal wheat disease detection by multi-spectral remote sensing", *Precision Agriculture*, 8(3): 161–172, 2007.

Franke, J., S. Gebhardt, G. Menz and H.P. Helfrich, "Geostatistical analysis of the spatiotemporal dynamics of powdery mildew and leaf rust in wheat", *Phytopathology*, 99: 974–984, 2009.

Galceran, E. and M. Carreras, "A survey on coverage path planning for robotics", *Robotics and Autonomous Systems*, 61(12): 1258-1276, 2013.

Gebbers, R. and V.I. Adamchuk, "Precision agriculture and food security", *Science*, 327(5967): 828–831, 2010.

Gennaro, S.F., L. Albanese, M. Benanchi, S.D. Marco, L. Genesio, A. Matese, et al.,

"An UAV-based remote sensing approach for the detection of spatial distribution and development of a grapevine trunk disease", in Proc. *8th International Workshop on Grapevine Trunk Diseases*, 734-737, 2012.

Glawe, D.A., L.J. Du Toit and G.Q. Pelter, "First report of powdery mildew on potato caused by Leveillula taurica in North America", Online, *Plant Health Progress*, 2004.

Glawe, D.A., T. Barlow, J.E. Eggers and P.B. Hamm, "First report of powdery mildew caused by Leveillula taurica of field-grown sweet pepper in the Pacific Northwest", Online, *Plant Health Progress*, 2010.

Hillnhuetter, C. and A.K. Mahlein, "Early detection and localisation of sugar beet diseases: new approaches", *Gesunde Pflanzen*, 60: 143–149, 2008.

Huang, Y.J. and F.F. Lee, "Classification of Phalaenopsis plantlet parts and identification of suitable grasping point for automatic transplanting using machine vision system", *Applied Engineering in Agriculture*, 24(1): 89-91, 2008.

Kavraki, L.E.and S.M LaValle, "Motion Planning", B. Siciliano and O. Khatib (Eds.), *Springer handbook of robotics*, Berlin: Springer-Verlag, 2008.

Kondo, N., K. Yata, M. Iida, T. Shiigi, M. Monta, M. Kurita and H. Omori, "Development of an End-Effector for a Tomato Cluster Harvesting Robot", *Engineering in Agriculture, Environment and Food*, 3(1): 20-24, 2010.

Kubota, C., M.A. McClure, N. Kokalis-Burelle, M.G. Bausher and E.N. Rosskopf, "Vegetable Grafting: History, Use, and Current Technology Status in North America", *HortScience*, 43: 1664-1669, 2008.

Lee W.S., V. Alchanatis, C. Yang, M. Hirafuji, D. Moshou and C. Li, "Sensing technologies for precision specialty crop production", *Computers and Electronics in Agriculture*, 74: 2-33, 2010.

Mann, M.P., D. Rubinstein, I. Shmulevich, R. Linker and B. Zion, "Motion planning of a mobile Cartesian manipulator for optimal harvesting of 2-D crops", *Transactions of the ASABE*, 57: 283-295, 2014.

Margaria, P., M. Ciuffo, M. Turina, "Resistance breaking strain of Tomato spotted wilt virus (Tospovirus; Bunyaviridae) on resistant pepper cultivars in Almeria Spain", *Plant Pathology*,53(6): 795, 2004.

McBratney, A., B. Whelan, T. Ancev and J. Bouma, "Future Directions of Precision Agriculture", *Precision Agriculture*, 6(1): 7-23, 2005.

Miranda, F.R., R.E. Yoder, J.B. Wilkerson and L.O. Odhiambo, "An autonomous controller for site-specific management of fixed irrigation systems", *Computers and Electronics in Agriculture*, 48: 183-197, 2005.

Monta, M., N. Kondo and H.C. Ting, "End-effector for Tomato Harvesting Robot", *Artificial Intelligence Review*, 12: 11-25, 1998.

Moshou, D., C. Bravo, R. Oberti, J.S. West, H. Ramon, S. Vougioukas, et al., "Intelligent multi-sensor system for the detection and treatment of fungal diseases in arable crops", *Biosystems Engineering*, 108(4): 311–321, 2011.

Nagasaka, Y., A. Mizushima, N. Noguchi, H. Saito and K. Kubayashi, "Unmanned rice-transplanting operation using a GPS-Guided rice transplanter with long mat-yype hydroponic seedlings", *Agriculture Engineering International*: *the CIGR*

Ejournal, 9, 2007.

Nutter, F.W.J., R.H. Littrell and T.B. Brennemann, "Utilization of a multispectral radiometer to evaluate fungicide efficacy to control late leaf spot in peanut", *Phytopathology*, 80: 102–108, 1990.

Oberti, R., P. Tirelli, M. Marchi, A. Calcante, M. Iriti and N.A. Borghese, "Automatic diseases detection in grapevine under field conditions", Pisa: Pisa University Press, 101-106, 2012.

Oberti, R., M. Marchi, P. Tirelli, A. Calcante, M. Iriti and A.N. Borghese, "Automatic detection of Powdery mildew on grapevine leaves by image analysis: Optimal view-angle range to increase the sensitivity", *Computers and Electronics in Agriculture*, 104: 1-8, 2014.

Oerke, E.C. and H.W. Dehne, "Safeguarding production losses in major crops and the role of crop protection", *Crop Protection*, 23: 275–285, 2004.

Otsu, N., "A Threshold Selection Method from Gray-Level Histograms", IEEE Transactions on Systems, Man, and Cybernetics, 9(1): 62-66, 1979.

Pagola, M., R. Ortiz, I. Irigoyen, H. Bustince, E. Barrenechea, P. Aparicio-Tejo, et al., "New method to assess barley nitrogen nutrition status based on image colour analysis", *Computers and Electronics in Agriculture*, 65(2): 213-218, 2009.

Parish, R.L., "Current developments in seeders and transplanters for vegetable crops", *HortTechnology*, 15: 346–351, 2005.

Patil, J.K., and R. Kumar, "Advances in image processing for detection of plant diseases", *Journal of Advanced Bioinformatics Applications and Research*, 2(2): 135-141, 2011.

Pernezny, K.L., P.D. Roberts, J.F. Murphy and N.P. Goldberg (Eds.), *Compendium of Pepper Diseases*, Wisconsin: American Phytopathological Society, 2003.

Pilli, S.K., B. Nallathambi, S.J. George, and V. Diwanji, "eAGROBOT- A Robot for Early Crop Disease Detection using Image Processing", in Proc. *IEEE International Conference on Electronics and Communication Systems*, 2014.

Pittman, H.A, "Spotted wilt of tomatoes, preliminary note concerning the transmission of the ‘spotted wilt’ of tomatoes by an insect vector (Thrips tabaci Lind.)", *Australian Journal Council for Science Industrial Research*, 1: 74-77, 1927.

Prins, M. and R. Goldbach, "The emerging problem of tospovirus infection and nonconventional methods of control", *Trends Microbiol*ogy, 6(1): 31-35, 1998.

Pujari, J.D., R. Yakkundimath, and A.S. Byadgi, "Image Processing Based Detection of Fungal Diseases in Plants", in Proc. *International Conference on Information and Communication Technologies*, 1802-1808, 2015.

Qiao, J., A. Sasao, S. Shibusawa, N. Kondo and E. Morimoto, "Mapping yield and quality using the mobile fruit grading robot", *Biosystems Engineering*, 90(2): 135-142, 2005.

Roggero, P., V. Masenga and L. Tavella, "Field isolates of Tomato spotted wilt virus overcoming resistance in pepper and their spread to other hosts in Italy", *Plant Disease*, 86(9): 950-954, 2002.

Rosella, S., M. Jose Diez and F. Nuez, "Viral diseases causing the greatest economic

losses to the tomato crop. I. The tomato spotted wilt virus- a review", *Scientia Horticulturae*, 67(3-4): 117-150, 1996.

Rumpf, T., A.K. Mahlein, U. Steiner, E.C. Oerke, H.W. Dehne, and L. Plümer, "Early detection and classification of plant diseases with Support Vector Machines based on hyperspectral reflectance", *Computers and Electronics in Agriculture*, 74(1): 91-99, 2010.

Ryu, K.H., G. Kim and J.S. Han, "AE- Automation and emerging technologies: Development of a robotic transplanter for bedding plants", *Journal of Agricultural Engineering Research*, 78: 141–146, 2001.

Sankaran, S., A. Mishra, R. Ehsani, and C. Davis, "A review of advanced techniques for detecting plant diseases", *Computers and Electronics in Agriculture*, 72(1): 1–13, 2010.

Savitzky, A., and M.J.E Golay, "Smoothing and Differentiation of Data by Simplified Least Squares Procedures", Analytical Chemistry, 36(8): 1627–1639, 1964.

Schellberg, J., M. Hill, R. Gerhards, M. Rothmund and M. Braun, "Precision agriculture on grassland: applications, perspectives and constraints", *European Journal of Agronomy*, 29: 59–71, 2008.

Schor, N., S. Berman, A. Dombrovsky, Y. Elad, T. Ignat and A. Bechar, "A robotic monitoring system for diseases of pepper in greenhouse", in Proc. *10th Euro. Conf. Precision Agriculture (ECPA)*, 627-634, 2015.

Schor, N., A. Bechar, T. Ignat, A. Dombrovsky, Y. Elad and S. Berman, "Robotic Disease Detection in Greenhouses: Powdery Mildew and Tomato Spotted Wilt Virus Identification", *IEEE Robotics and Automation Letters* with *IEEE International Conference on Robotics and Automation*, submitted for publication.

Schor, N., S. Berman, A. Dombrovsky, Y. Elad, T. Ignat, and A. Bechar, "Perception apparatus design for a robotic system for greenhouse pepper disease detection", *Precision Agriculture*, submitted for publication.

Sharman, M. and D.M. Persley, "Field isolates of Tomato spotted wilt virus overcoming resistance in Capsicum in Australia", *Australasian Plant Pathology*, 35(2): 123-128, 2006.

Smith, R., S.T. Koike, M. Davis, K. Subbarao and F. Laemmlen, "Several fungicides control Powdery mildew in peppers", *California Agriculture*, 53(6): 40–43, 1999.

Stafford, J.V. "Implementing precision agriculture in the 21st Century", *Journal of Agricultural Engineering Research*, 76: 267–275, 2000.

Steiner, U., K. Bürling and E.C. Oerke, "Sensor use in plant protection", *Gesunde Pflanzen*, 60: 131–141, 2008.

Tirelli, P., M. Marchi, A. Calcante, S. Vitalini, M. Iriti, N.A. Borghese and R. Oberti, "Multispectral image analysis for grapevine diseases automatic detection in field conditions", in Proc. *International conference of agricultural engineering CIGR*, 1-6, 2012.

Van Henten, .E.J., B.A.J. Van Tuijl, G.J. Hoogakker, M.J. Van Der Weerd, J. Hemming, J.G. Kornet and J. Bontsema, "An autonomous robot for deleafing cucumber plants grown in a high-wire cultivation system", Biosystems Engineering, 94: 317–323, 2006.

Van Henten, E.J., D.A. Van’t Slot, C.W.J. Hol and L.G. Van Willigenburg, "Optimal manipulator design for a cucumber harvesting robot", *Computers and electronics in agriculture*, 65(2): 247-257, 2009.

Vijayakumar J. and S. Arumugam, "Recognition of Powdery Mildew Disease for Betelvine Plants Using Digital Image Processing", *International Journal of Distributed and Parallel Systems (IJDPS)*, 3(2), 2012.

Zheng, Z., T. Nonomura, M. Appiano, S. Pavan, Y. Matsuda, H. Toyoda, et al., "Loss of function in mlo orthologues reduces susceptibility of pepper and tomato to Powdery mildew disease caused by Leveillula taurica", *PLoS ONE*, 8(7), 2013.

מילות מפתח

אוטומציה בחקלאות, ראייה ממוחשבת לאוטומציה, מערכת רובוטית לזיהוי מחלות, זיהוי מחלות, נגיף כתמי הנבילה של העגבנייה, קמחונית, סיווג, ניתוח גורמים ראשיים, מקדם השונות, גידול פלפל בחממות.

תקציר

מערכות רובוטיות לזיהוי מחלות בצמחים בחממות מאפשרות גילוי מוקדם של המחלות ומשפרות את הבקרה עליהן. מערכות אלו צפויות להגדיל את התפוקה, לשפר את האיכות, להפחית שימוש בחומרי הדברה, להגדיל את הקיימות ולהפחית את העלויות. לכל מחלה תסמינים שונים ביבולים שונים וכל צמח רגיש למספר רב של מחלות, לכן נדרשים אלגוריתמים ייעודים לזיהוי כל מחלה בכל יבול. אנו מציגים מערכת רובוטית לזיהוי מחלות בחממת פלפל שפותחה תחת גישה הוליסטית, המשלבת את תכן מנגנוני התנועה והתפיסה, למטרת זיהוי שתי מחלות עקריות ונפוצות בחממות פלפל: קמחונית (powdery mildew) ונגיף כתמי הנבילה של העגבנייה (*Tomato spotted wilt virus* - TSWV). המערכת הרובוטית לזיהוי המחלות כוללת מבנה מכאני, סט חיישנים, אלגוריתמים לתכנון תנועה ואלגוריתמים לזיהוי מחלות. תמונות בערוצי הספקטרום הנראה (אדום, ירוק וכחול) משמשות לתכנון תנועה וזיהוי מחלות, לשם פעולה מהירה, חסכונית ולא הרסנית. לזיהוי קמחונית פותח אלגוריתם מבוסס על ניתוח גורמים ראשיים (principal component analysis - PCA), ושלושה אלגוריתמים פותחו לזיהוי נגיף כתמי הנבילה של העגבנייה, אחד מבוסס על PCA ושניים מבוססים על מקדם השונות (coefficient of variation - CV). האלגוריתמים נבדקו באמצעות תמונות של צמחי פלפל בריאים וחולים שצולמו בחממה. עבור צילום צבע (RGB), לזיהוי נגיף כתמי הנבילה של העגבנייה אלגוריתם סיווג המבוסס על PCA עם הסרת ורידי העלה, השיג דיוק גבוה ביותר (90%), עם זאת הדיוק של אלגוריתמי הסיווג המבוססים על CV היה גבוה גם כן (85%, 87%). לזיהוי קמחונית, דיוק הסיווג ברמת הפיקסל היה גבוה (95.2%), ואילו דיוק הסיווג ברמת העלה היה נמוך (64.3%) כיוון שהתמונות שצולמו ונותחו היו של החלק העליון של העלה בעוד שתסמיני המחלה מופיעים בחלק התחתון של העלה. צילום מולטיספקטרלי, עבור שתי המחלות, השיג תוצאות נחותות מאלו שהושגו בצילום צבע. רכיבי המערכת שולבו ובדיקות אינטגרציה ראשוניות נערכו במעבדה כדי לוודא שכל רכיבי המערכת אכן פועלים בתיאום. המערכת השלמה פעלה בהצלחה במשך 110 דקות רצופות עם זמן מחזור ממוצע של 26.7 שניות עבור מהירות יחידת הקצה של 15 מ״מ/שניה ואלגוריתמי סיווג מבוססי PCA. מחקר המשך יבחן שיפור של אלגוריתמי זיהוי המחלות, לדוגמא את השילוב של שתי שיטות הסיווג המבוססות על CV, וכן יבחן לעומק את פעולת המערכת הכוללת כולל פעולה עם תנועה של הצמח הנבחן ביחס למערכת הרובוטית, וכן תבוצע בדיקה מקיפה של המערכת בחממה (בתנאי שדה).

אוניברסיטת בן-גוריון בנגב
הפקולטה למדעי ההנדסה
המחלקה להנדסת תעשייה וניהול

מערכת רובוטית לזיהוי מחלות בחממת פלפל

חיבור זה מהווה חלק מהדרישות לקבלת תואר מגיסטר בהנדסה

מאת: נעה שור

מנחים: סיגל ברמן
אביטל בכר

מחברת:	תאריך: .....
מנחים:	תאריך: .....
.....	תאריך: .....
יו"ר ועדת תואר שני מחלקתית:	תאריך: .....

תשרי תשע"ו — אוקטובר 2015

אוניברסיטת בן-גוריון בנגב
הפקולטה למדעי ההנדסה
המחלקה להנדסת תעשייה וניהול

מערכת רובוטית לזיהוי מחלות בחממת פלפל

חיבור זה מהווה חלק מהדרישות לקבלת תואר מגיסטר בהנדסה

מאת: נעה שור

תשרי תשע"ו אוקטובר 2015